

Thioarsenides: a case for long-range Lewis acid–base-directed van der Waals interactions

G. V. Gibbs · A. F. Wallace · R. T. Downs ·
N. L. Ross · D. F. Cox · K. M. Rosso

Received: 29 April 2010 / Accepted: 9 September 2010
© Springer-Verlag 2010

Abstract Electron density distributions, bond paths, Laplacian and local-energy density properties have been calculated for a number of As_4S_n ($n = 3, 4$ and 5) thioarsenide molecular crystals. On the basis of the distributions, the intramolecular As–S and As–As interactions classify as shared bonded interactions, and the intermolecular As–S, As–As and S–S interactions classify as closed-shell van der Waals (vdW) bonded interactions. The bulk of the intermolecular As–S bond paths link regions of locally concentrated electron density (Lewis-base regions) with aligned regions of locally depleted electron density (Lewis-acid regions) on adjacent molecules. The paths are comparable with intermolecular paths reported for several other molecular crystals that link aligned Lewis base and acid regions in a key–lock fashion, interactions that classified as

long-range Lewis acid–base-directed vdW interactions. As the bulk of the intermolecular As–S bond paths ($\sim 70\%$) link Lewis acid–base regions on adjacent molecules, it appears that molecules adopt an arrangement that maximizes the number of As–S Lewis acid–base intermolecular bonded interactions. The maximization of the number of Lewis acid–base interactions appears to be connected with the close-packed array adopted by molecules: distorted cubic close-packed arrays are adopted for alacránite, pararealgar, uzonite, realgar and β -AsS and the distorted hexagonal close-packed arrays adopted by α - and β -dimorphite. A growth mechanism is proposed for thioarsenide molecular crystals from aqueous species that maximizes the number of long-range Lewis acid–base vdW As–S bonded interactions with the resulting directed bond paths structuralizing the molecules as a molecular crystal.

G. V. Gibbs (✉) · N. L. Ross
Departments of Geosciences, Materials Science and Engineering
and Mathematics, Virginia Tech, Blacksburg, VA 24061, USA
e-mail: ggibbs@vt.edu

A. F. Wallace
Earth Science Division, Lawrence Berkeley National
Laboratory, Berkeley, CA 94720, USA

R. T. Downs
Department of Geosciences, University of Arizona,
Tucson, AZ 85721, USA

D. F. Cox
Department of Chemical Engineering, Virginia Tech,
Blacksburg, VA 24061, USA

K. M. Rosso
Chemical and Materials Science Division,
W.R. Wiley Environmental Molecular Sciences Laboratory,
Pacific Northwest National Laboratory,
Richland, WA 99352, USA

Keywords Realgar · Pararealgar · Dimorphite · Uzonite · Alacránite

Introduction

Van der Waals (vdW) interactions are commonly believed to comprise the weak, long range, noncovalent and largely nondirectional interactions that occur among atoms, molecules and membranes that structuralize nanomaterials, graphite, fullerenes, sheet silicates like talc and pyrophyllite and molecular crystals. There are three well-known types of vdW interactions (excluding intermolecular hydrogen bonding): Keesom type (permanent dipole–dipole interactions), Debye type (permanent dipole-induced dipole interactions) and London dispersion type (induced dipole-induced dipole interactions between nonpolar aggregates). On the basis of the nonlocalized central bonded interactions,

the molecules of organic molecular crystals may be expected to fill space as efficiently as possible, adopting a variant of a cheek-by-jowl dense close-packed array of molecules (Kitaigorodskii 1955; Dunitz and Gavezzotti 2005, 2009). In contrast, Kitaigorodskii (1955) asserted, on the basis of a survey of a relatively large number of experimentally determined inorganic molecular structures, that directional forces play a more determinative role in the structuralization of inorganic molecular crystals. In addition to the structuralization of nanomaterials and organic and inorganic molecular crystals, vdW interactions are believed to play a fundamental role in processes involving gases and liquids (Maitland et al. 1980), proteins and drug interactions (Lauria et al. 2009), catalysts and substrate interactions (Mikami et al. 1994), the folding of membrane-embedded proteins (Fiedler et al. 2010), the self-assembly of nanomaterials (Wei et al. 2009), the aromatic stacking of nucleic acid bases (Sponer et al. 2008), the conformation analysis of nucleic acids and proteins (Dovbeshko et al. 2009), tribology—the friction interactions between surfaces (Feldman et al. 1998), dispersive adhesion and particle–surface interactions (Gotzinger and Peukert 2003) and the froth flotation of ores and oxides (Xu et al. 2009).

But the modeling of these processes in terms of nondirectional vdW interactions has been a difficult and thorny issue, particularly for cases where the interactions are poorly understood and difficult to characterize (Gotzinger and Peukert 2003), mainly given the inadequacy of the theories of polar and electrostatic interactions (French et al. 2010). The difficulties encountered by Zallen et al. (1971), for example, in the vdW modeling of the rigid interlayer Raman-infrared spectral modes for orpiment, As_2S_3 , led to the conclusion that “The assumption of van der Waals forces is often made in the absence of better information and is an admission of ignorance about the detailed nature of the intermolecular interaction.” In point of fact, the experimental Raman and infrared spectra for the chalcogenide clearly established that the neutral layers of the structure are linked by directed interlayer vdW bonded interactions. Further, vibrational modes and the dispersion of the low-frequency modes have also been used to establish the character of the vdW interchain forces in trigonal selenium (Martin et al. 1976). In particular, the dispersion of the experimental low-frequency modes clearly demonstrates that the trigonal chains of Se atoms are likewise linked by directed (covalent) vdW interchain forces. These important examples demonstrate that directed vdW forces play an important role in the structuralization of the sheets in orpiment and the chains in trigonal selenium as expected for inorganic molecular materials (Kitaigorodskii 1955). The question that comes to mind is ‘How common are these vdW-directed forces, and how are they related to the distribution of the electron density?’

As the detailed nature of a vdW force may be expected to be embodied in the electron density (ED) distribution, Feynman (1939) undertook a careful study of the ‘forces in molecules’ and found that vdW forces can be interpreted in terms of the accumulation of the ED distribution between the nuclei of a pair of bonded atoms. Using equations formulated to evaluate the forces directly for a pair of bonded atoms at a separation, R , large compared with the radius sum for the pair of atoms, he not only found that the ED distribution for each of the atoms is deformed from central symmetry, but that a dipole moment is induced on each with the center of gravity of the ED distribution for the pair displaced slightly toward one another. On the basis of this result, he concluded that “It is not the interaction of these dipoles which leads to van der Waals forces, but rather the attraction of each nucleus for the distorted charge distribution of its own electrons that gives the attractive $1/R^7$ force.” In effect, he showed that the semi-classical interpretation of dispersion ascribed to the interaction of oscillating dipoles on two adjacent molecules or to induced dipoles maybe without basis for a pair of vdW bonded atoms. Moreover, on the basis of the accumulation of the ED between the pair and the connection between the Hellmann–Feynman and the virial theorems and covalent binding, Slater (1972) went a step further and concluded ‘that there is no very fundamental distinction between van der Waals binding and covalent binding.’

In a recent derivation of the exchange–correlation potential corresponding to the nonlocal vdW functional for a geometry optimized noble gas pair of argon atoms, Thonhauser et al. (2007) found that the ED migrates from around the nuclei to the region between the vdW bonded atoms, a result that explains the ‘strong binding’ of the Ar_2 noble gas dimer. The resulting binding energy and forces were found to change considerably with the accumulation of the ED between the pair of atoms. On the basis of this result, it was concluded that “This is the van der Waals analog of the covalent bond, although it is much weaker” as asserted earlier by Slater (1972). Given these observations, it is not surprising that the argon atoms are connected by a bond path (a line of maximum electron density that connects the nuclei of bonded atom) with an accumulation of the ED at the bond critical point of $0.64 \text{ e}/\text{\AA}^3$ [the point along the bond path between the nuclei of bonded pair of atoms where the ED is a minimum (Bader and Essén 1984)]. Further, the accumulation of the ED between the nuclei is consistent with Feynman’s (1939) conclusion that it is not the interaction of dipoles that results in the vdW forces, but rather the attraction of the nuclei for the accumulation of the ED in the binding region that results in the vdW forces. Further, the greater the accumulation of the ED in the binding region, usually the shorter the bonded interaction.

With the tacit assumption of a covalent vdW bonded interaction, an intermolecular interaction in a molecular crystal may be considered to have directional character in the sense that a covalent bond has direction. If so, then it is logical to deduce that there is a continuum of directed bonded interactions that exist in molecular crystals between covalent and vdW interactions (Slater 1972). Further, similar trends are anticipated between the bond length and the accumulation of the ED between given pairs of intermolecular and intramolecular bonded atoms. On the basis of these conclusions, Bader (1990) asserted that the forces that determine the structures of the molecules in a molecular crystal are no different from those that determine the intermolecular bonded interactions between the molecules. He also concluded that the accumulation of the ED between the nuclei for a bonded pair of atoms naturally results in a line of maximum ED, a line that in effect may correspond with the direction of the bonded interaction, an interaction that is considered to play a decisive role in structuralizing the molecules in a molecular crystal (Bader 1998, 2009; Bone and Bader 1996). The ED distribution and its topological properties are not only expected to reveal features that are comparable with those found by Feynman (1939) but also to provide new insight into the features of the ED that is expected to provide a new approach to understanding vdW bonded interactions in molecular crystals in terms of the electrostatic properties of the ED distribution. Such a connection is anticipated between the two given that the ED distribution contains all of the information that can be measured for the material, including its kinetic, potential and total energy (Parr and Yang 1989).

To provide the nonspecialist reader with an appreciation of a bond path in terms of the ED distribution, bond paths were tracked in the calculation of envelopes of constant ED for four representative As_4S_4 molecules extracted from the pararealgar molecular structure (Fig. 1). The arsenic and sulfur atoms occur at the respective green and yellow corners of each molecular graph (the network of bond paths that link neighboring bonded nuclei) of the molecules depicted in Fig. 1a. The envelopes of constant ED are displayed in Fig. 1b. The dark gray envelope was calculated at the $0.35 \text{ e}/\text{\AA}^3$ level, and the light gray one that encloses the dark gray one was calculated at the $0.05 \text{ e}/\text{\AA}^3$ level. The dark envelope not only encloses each of the atoms of the molecules, but it also forms single-sheeted hyperboloidal-shaped envelopes that connect each of the bonded atoms, defining the intramolecular bond paths. The light grey envelope surface not only completely encloses the intramolecular envelope, but it also encloses each of the intermolecular bond paths. The directions of the intermolecular vdW bond paths are depicted by the red lines in Fig. 1b. It is

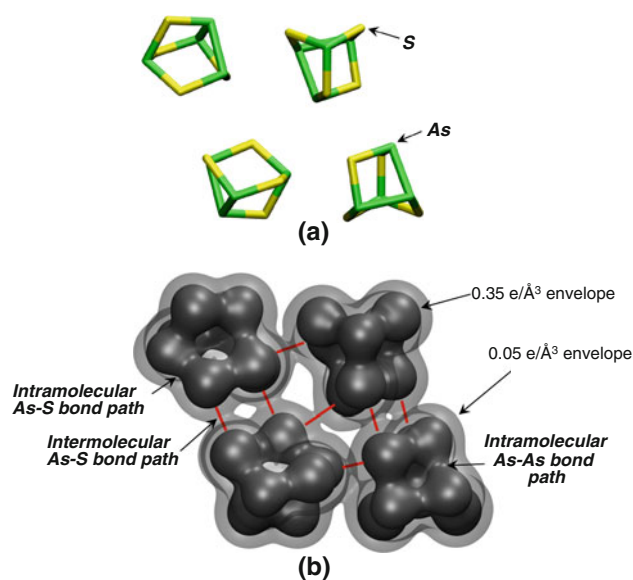


Fig. 1 Intramolecular and intermolecular van der Waals bond path for four As_4S_4 molecules in pararealgar. **a** The green corners of the molecular graphs define the positions of the arsenic atoms and the yellow ones define positions of the sulfur atoms. Envelopes of the electron density distributions, $\rho(\mathbf{r})$, calculated for the four molecules are displayed in **b**. The dark gray envelope of $\rho(\mathbf{r})$ is mapped at the $0.34 \text{ e}/\text{\AA}^3$ level, and light gray envelope is mapped at the $0.05 \text{ e}/\text{\AA}^3$ level. Because of the larger value of $\rho(\mathbf{r}) = 0.34 \text{ e}/\text{\AA}^3$ of the dark gray envelope, the envelope is situated closer to the nuclei of the atoms of the molecules. The dark envelope encloses each of the atoms and extend along each the intramolecular As–S and As–As bond paths as a single-sheeted hyperboloidal-shaped envelope of $\rho(\mathbf{r})$ to the coordinating atoms. The calculated $\rho(\mathbf{r}_c)$ values for the As–S and As–As bonded interactions are ~ 0.65 and $\sim 0.45 \text{ e}/\text{\AA}^3$, respectively, both larger than the value of the dark gray envelope. As the light gray envelope was calculated at the $0.05 \text{ e}/\text{\AA}^3$ level; it necessarily encloses the dark gray envelope. The calculated $\rho(\mathbf{r}_c)$ values for the intermolecular As–S and As–As bond paths both range between ~ 0.05 and $0.08 \text{ e}/\text{\AA}^3$, values close to the value of the light gray envelope. The intermolecular As–S and As–As bond paths are drawn in red and are enclosed by the envelopes that connect the atoms on adjacent molecules. The intramolecular and intermolecular van der Waals hyperboloidal-shaped envelopes are in effect pictures of the electron density that enclose the lines of maximum electron density that connected the bonded atoms

evident from these maps that vdW intermolecular bond paths exist between each of the molecules of the pararealgar molecular crystal. Of equal importance, it is also evident, as concluded by Feynman (1939), that vdW interactions arise by dint of the accumulation of the ED between the nuclei of the bonded atoms rather than by dint of dipole–dipole interactions. It is important to bear in mind that bond paths are not chemical bonds but regions of maximum ED that bridge the bonded atoms as emphasized by Bader (2009). Further, as claimed by Bader (2010), there are no known instances of a bonded interaction being generated in the absence of a corresponding bond path.

Earlier studies of Lewis acid–base-directed van der Waals interactions

Until recently, relatively few studies had been completed for inorganic molecular crystals in terms of the topological properties of their ED distributions. As such, comparatively little has been established about the role played by directed bonded interactions and the connection between the intermolecular bond paths, aligned Lewis acid–base regions and packing considerations. The molecular crystals examined, to date, include solid molecular chlorine, Cl_2 (Tsirelson et al. 1995), chlorinefluoride (Boese et al. 1997), tetrasulfur tetranitride (Scherer et al. 2000), s enarmontite, Sb_4O_6 (Whitten et al. 2004), arsenolite, As_2S_3 (Gibbs et al. 2009) and tetraoxide dinitride (Tsirelson et al. 2009). Collectively, these studies serve as examples where directed intermolecular bond paths radiate from one molecule to another, serving as what has been considered to be ‘key–lock’ Lewis acid–base mainstays in the structuralization of the molecules in the crystals (Scherer et al. 2000).

In this report, the studies undertaken for solid chlorine and arsenolite will be reviewed inasmuch as the features of the ED distribution. The alignment of the Lewis acid–base regions associated with the bond paths for these materials are comparable with those reported for the other molecular crystals. Solid chlorine was chosen in particular because its molecules are disposed in layers in a more or less close-packed array where each Cl_2 molecule is coordinated by ten equivalent Cl_2 molecules. In contrast, arsenolite was chosen because each of its molecules is coordinated by four equivalent molecules, occupying about one-third of the space that would be occupied by a close-packed structure. The study of the ED for the two structures and their ED distributions affords an opportunity to compare the intermolecular bonded interactions and their associated bond paths for structures with sharply contrasting molecular packing properties.

Solid molecular chlorine

To our knowledge, the experimental structure of solid chlorine has yet to be reproduced using a nondirectional pair-wise Lennard-Jones (12–6) vdW central potential (Hillier and Rice 1967; Nyburg 1964). The modeling of the structure in terms of the pair-wise potential results in a nonplanar structure with the ends of the individual Cl_2 molecules in one layer disposed in a staggered configuration with respect to the ends of the molecules in the adjacent layers. As the molecules in the observed structure are not staggered but lie in a common plane, it was concluded that solid chlorine is not a simple vdW structure (Williams and Hsu 1985). However, when the Lennard-Jones potential was modified with a directed partial bonded force

constant term, they found that the structure can be reproduced within the ‘threshold of accuracy’.

With the success of the directed force constant model, Tsirelson et al. (1995) undertook a careful examination of the topology of the ED distribution to explore whether the structure might be understood in terms of the alignment of regions of local concentrated and depleted ED as defined by the Laplacian operator, $L(\mathbf{r}) = -\nabla^2\rho(\mathbf{r})$. In the study, they optimized the geometry for a pair of Cl_2 molecules, using a relatively robust MP2 6-311++G(2d) basis set. The optimized geometry for the pair was found to be comparable with that observed for the pair in the crystal, possessing an intermolecular Cl–Cl distance of 3.37   and a shorter intramolecular distance of 2.03  , compared with those observed for the crystal of 3.32 and 1.97  , respectively. Clearly, the relatively short intramolecular Cl–Cl distance is comparable with that observed for the crystal. Moreover, the observed intermolecular distance is somewhat smaller than the sum of the corresponding vdW radii, 3.50  , as may be expected for a bonded interaction (Carroll and Bader 1988). They reported that the pair of bonded Cl_2 molecules was stabilized by 7.6 kcal/mol relative to two noninteracting Cl_2 molecules, providing a measure of the vdW reaction energy for two noninteracting molecules.

The mapping of the Laplacian, $L(\mathbf{r})$, for the pair of Cl atoms, calculated at a constant value of -2.5 a.u., resulted in a spherical envelope (colored red in Fig. 2) enclosing each Cl atom, defining a region where the ED has been locally depleted (Tsirelson et al. 1995). A mapping at the $+2.0$ a.u. value resulted in a silver torus-shaped envelope surrounding each Cl, each oriented perpendicular to the bond path and defining a region where the ED is locally concentrated. The region of locally concentrated ED, enclosed by the torus-shaped envelope, represents a Lewis-base region (a nucleophile) while that of locally depleted

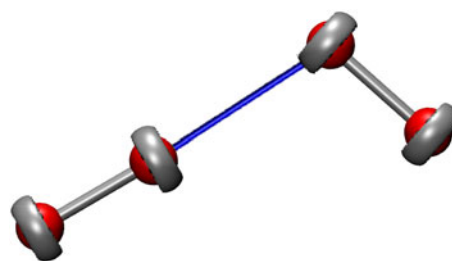


Fig. 2 Laplacian $L(\mathbf{r}) = -\nabla^2\rho(\mathbf{r})$ envelope map for two geometry optimized chlorine molecules (after Tsirelson et al. 1995). The intramolecular bond paths are colored silver, and the intermolecular path is colored blue. The nucleus of each the Cl atoms is enclosed by a spherical $L(\mathbf{r}) = -2.0$ a.u. red envelope which in turn is surrounded by a $L(\mathbf{r}) = +2.5$ a.u. silver torus-shaped envelope. The electron density is locally concentrated within the torus-shaped envelope (a Lewis base), and it is depleted within the red envelope (a Lewis acid)

ED, enclosed by the red sphere, represents a Lewis-acid region (an electrophile). As observed by Bader et al. (1988), a Lewis acid–base type interaction typically corresponds to the combination of a nucleophilic region of locally concentrated ED with an electrophilic region of locally depleted ED with the concomitant formation of a bond path connecting the regions and a concomitant bonded interaction. Figure 2 displays the intermolecular bond path that connects the Lewis acid sphere of one Cl atom of the Cl₂ dimer with the Lewis torus-shaped region enclosing a Cl atom on the second dimer, a manifestation of a Lewis base–acid type interaction that has occurred between the two dimers with the concomitant formation of a bond path and a vdW bonded interaction connecting the pair as a (Cl₂)₂ complex. As the magnitude of the local concentration of the ED associated with the torus-shaped Lewis-base region together with the depth of local depletion of the ED associated with spherical-shaped Lewis-acid region about the Cl are relatively large, it is apparent that the interaction between the two molecules is nontrivial and that the pair is linked by a well-defined long-range Lewis acid–base-directed closed-shell bonded interaction, a result that is consistent with the Williams and Hsu (1985) directed force constant model. Further, the two regions of localized ED at the ends of both Cl₂ molecule may be considered to correspond with the dipoles in the ED reported in the study of the forces for a molecule (Feynman 1939).

A mapping of $L(\mathbf{r})$ for the atoms in the (100) plane for solid chloride (Fig. 3) reveals that each Cl₂ molecule displays an array of features that is comparable with that determined for the pair of Cl₂ molecules (Fig. 2). The map shows that each Cl atom is surrounded by a torus-shaped

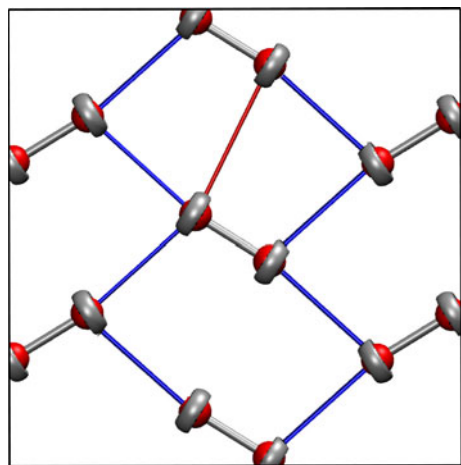


Fig. 3 $L(\mathbf{r})$ envelope map for solid chlorine for the Cl₂ molecules lying in the (100) plane (after Tsirelson et al. 1995). The bond paths that connect the silver Lewis base torus-shaped envelopes with the red Lewis acid spherical envelopes are colored blue, and the path that connects the silver Lewis base torus-shaped envelopes is colored red. The $L(\mathbf{r})$ values and envelopes are given in legend of Fig. 2

Lewis-base region oriented perpendicular to the long axis of the molecule with a spherical Lewis-acid region of locally depleted ED enclosing the atom. It also shows that the molecules are oriented in a specific way such that each acid region is aligned with a base region, the sort of alignment that is associated with a Lewis acid–base bonded interaction (Bader and MacDougall 1985) as found for the optimized pair of Cl₂ molecules. As observed by Bader (1990), this alignment corresponds to the combination of a region of excess potential energy (base region) with one of excess kinetic energy (acid region) to yield a bonded pair of atoms for which the virial theorem is satisfied. A calculation of the ED distributions for the molecules also reveals that the base and acid regions interact and form a well-developed directed bond path between the two regions depicted by the blue lines in Fig. 3. In effect, the formation of the bond path may be considered to correspond to a long-range intermolecular Lewis base–acid type chemical interaction involving the combination of a nucleophile and an electrophile (Pine and Hendrickson 1980).

As such, the acid regions may be considered to be connected to the base regions on adjacent molecules via directed bond paths as may be expected on the basis of the directed character of the interaction (Slater 1972). The aligned Lewis base–acid regions and their connecting directed bond paths are repeated throughout the structure, resulting in a periodic molecular array of Cl₂ molecules, connected by sets of directed bond paths (see Fig. 4c; Tsirelson et al. 1995). A second set of bond paths connect the adjacent torus-shaped Lewis-base regions (red line in Fig. 3). In this case, the two regions of local charge concentration are considered to interfere constructively and form the bond path connecting two Lewis-base regions, resulting in a local concentration of ED between the pair of Cl atoms. Together, the acid–base and base–base regions connected by bond paths are concluded to serve as directed mainstays that govern and structuralize the spatial array of the Cl₂ molecules in a key–lock fashion. The Lewis base–base interactions are considered to be the weaker of the two interactions given that the Cl–Cl base–base bond path length, 3.83 Å, is longer than the Cl–Cl acid–base bond path length, 3.32 Å. As observed by Bader (1998), by dint of the presence of the acid–base and base–base bond paths in the solid, molecular chlorine forms parallel relatively ‘close-packed’ monolayers of Cl dimers paralleling (100) where each dimer is coordinated by ten neighboring dimers. The conformity of the structure with Kitaigorodsky’s (1973) Aufbau rule suggests that directed closed-shell intermolecular bonded interactions can result in an arrangement of molecules that fill space in a relatively close-packed fashion governed by directed bonded interactions. It is notable that the $L(\mathbf{r})$ envelope maps for the two Cl₂ molecules (Fig. 2) are virtually the same as those in solid chlorine (Fig. 3),

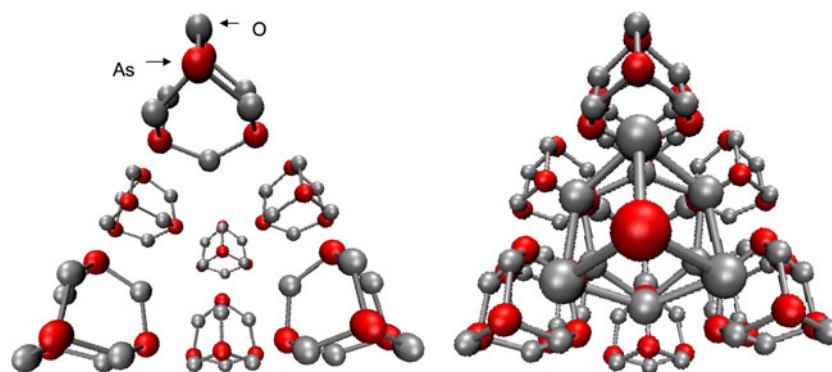


Fig. 4 Two perspective drawings of moieties of the structure of arsenolite, As_2O_3 , viewed down [110]. The *red spheres* represent As atoms, and the *silver* ones represent O atoms. The intramolecular bond paths connecting the As and S atoms are colored *silver*. The barycenter of the central molecule is at a fractional height of 0.125,

the ones at 2, 6 and 10 o' clock are each at height of 0.375, and the ones at 4, 8 and 12 o'clock are each at a height of 0.625. The drawing on the *right* differs from the one on the *left* in that an extra molecule is added topping the one on the *right*

reflecting the little impact that the local field of Cl_2 molecules has on the envelopes of the individual molecules. As expected, there is absence of intermolecular bond paths in the structure, connecting the acid regions by dint of the local depletion of ED in these regions.

Arsenolite

The ED distribution, the bond critical point and the local-energy density properties and $L(\mathbf{r})$ isosurfaces have likewise been calculated for arsenolite (As_2O_3) (Gibbs et al. 2009) to establish whether a connection exists between the bond paths and the Lewis-acid regions on the As atoms and Lewis-base regions of the O atoms. A perspective drawing of a representative block of the structure is displayed in Fig. 5. A mapping of the barycenters for the molecules shows that the individual molecules are arranged like the C atoms in diamond (Bozorth 1923), establishing that the As_4O_6 molecules occupy about one-third of the space that would be occupied by a close-packed array of molecules. To learn whether the open structure can be understood in terms of directed bond paths, the ED distribution for the arsenolite was calculated, the positions of bond critical points were located, and the bond paths were tracked. Pictures of the As_4O_6 molecules, with the resulting intermolecular As–O and O–O bond paths, each radiating from two of the tetrahedral faces of centrally located molecules to the tetrahedral faces of two adjacent equivalent molecules, are displayed in Fig. 5a, b, respectively. The intermolecular As–O bond paths are colored blue, while the intramolecular ones are silver. The O–O paths are pink. Figure 5c displays a representative central As_4O_6 molecular moiety with a set of As–O bond paths radiating from three of its four tetrahedral faces to the tetrahedral faces of three adjacent molecules. In effect, each molecule in

arsenolite is coordinated by four equivalent As_4O_6 molecules disposed at the corners of a tetrahedron, the periodic repetition of the pattern displayed in Fig. 5a, b, resulting in an open tetrahedral structure of molecules. Clearly, the molecules in arsenolite are not close-packed, with the bumps of one molecule filling the hollows of adjacent molecules (Dunitz and Gavezzotti 2005). Instead, the four faces of each molecule are juxtaposed with the faces of four adjacent molecules, forming a tetrahedral array of molecules. The bond paths that connect the molecules together in an open tetrahedral structure provide a basis for understanding the structure in terms of the directed intermolecular bonded interactions. Figure 6 displays a composite envelope $L(\mathbf{r})$ map superimposed on the arsenolite structure viewed down [110]. Each As atom is enclosed by a spherical envelope generated at a $L(\mathbf{r}) = -22$ a.u.; this value represents a region of charge depletion (an acid region) with a skull cap-shaped envelope of modestly concentrated ED, $L(\mathbf{r}) = 0.01$ a.u., located at the apex of each As atom forming the so-called ψ - AsO_3 tetrahedra that comprise the As_4O_6 molecule. In contrast, each O atom is encircled in part by a ear muff-shaped Lewis-base region located on the reflex side of each As–O–As angle with a much larger $L(\mathbf{r})$ value of +12 a.u. Intermolecular As–O bond paths branch from the spherical Lewis-acid regions that encircle each As atom to the ear muff-shaped Lewis-base region on an O atom of an adjacent molecule, qualifying as a long-range Lewis acid–base-directed bond path interaction. Figure 7 displays the same composite $L(\mathbf{r})$ envelope map displaying the intermolecular O–O bond paths that connect the ear muff-shaped Lewis-base regions on the O atoms on adjacent molecules, qualifying as Lewis base–base bonded interactions. Collectively, the As–O Lewis acid–base and the O–O Lewis base–base-directed bond paths may be considered to serve as

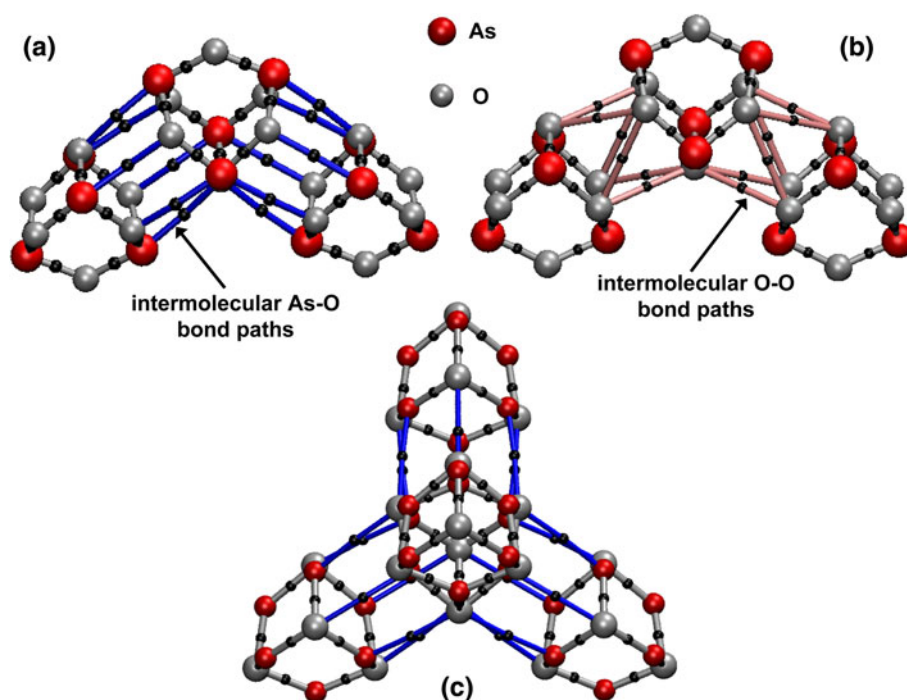


Fig. 5 The As_4O_6 molecules in arsenolite connected by intramolecular As–O and O–O bond paths. The As atoms are colored *red*, the O atoms are colored *silver*, the O–O bond paths are colored *pink*, the As–O paths are colored *blue*, and the bond critical points are represented by small *black dots* located along the bond paths: **a** an As_4O_6 molecule coordinated by two As_4O_6 molecules with O–O bond paths radiating from the tetrahedral surfaces of the central molecule. The angle between the barycenter of the central molecule and the barycenters of the two coordinating molecules is $\cos^{-1}(-1/3)$, **b** an

As_4O_6 molecule coordinated by two As_4O_6 molecules with As–O bond paths radiating from the tetrahedral surfaces of the central molecule to two coordinating molecules and **c** an As_4O_6 molecule coordinated by three As_4O_6 molecules with As–O bond paths radiating from the tetrahedral surfaces of the central molecule. Each molecule in the arsenolite structure is tetrahedrally coordinated by four equivalent molecules, resulting in a cubic crystal with $Fd\bar{3}m$ space group symmetry

‘key–lock’ Fischer mainstays (Bader et al. 2007), providing a basis for understanding the open tetrahedral structure adopted by arsenolite. However, unlike solid chlorine, the bond path length between the intermolecular O atoms is shorter, 3.02 Å, than those between the intermolecular As and O atoms, 3.05 Å. It is notable that in the case of *sénarmontite* that each Sb_4O_6 molecule is coordinated by four equivalent molecules like those in the topologically equivalent arsenolite structure. In a careful study of the topology of the ED distribution, Whitten et al. (2004) found that Sb–O bond paths connect the acid regions of the antimony atoms *sénarmontite* with the lone pair base regions on the O on adjacent molecules. But, unlike arsenolite, O–O intermolecular bond paths are absent. Further, on the basis of electrostatic potential maps calculated for the Sb_4O_6 molecule, the alignment of the positive and negative surfaces of the envelope maps together with the directed Sb–O bond paths made it clear why the molecules adopt a ‘key–lock’ arrangement: the regions of negative potential of one molecule overlap the regions of positive potential on adjacent molecules with the directed Sb–O bond paths connecting the tetrahedral faces of the molecules (Whitten et al. 2004).

Similar to the system of directed bond paths displayed for arsenolite, the molecular As_2O_3 molecular sheets of *claudetite* I and II are linked together by weak As–O-, O–O- and As–As-directed bonded interactions (Gibbs et al. 2009). Moreover, the highly corrugated nature of the sheets in *claudetite* II are associated with intermolecular As–O bond paths and bonded interactions within the layers connecting the base regions on the O atoms and the acid regions on the As atoms. The arrangement of the As atoms in the two *claudetite* polymorphs is similar to those in native bulk arsenic where comparable corrugated sheets consisting of three-coordinated As atoms are linked together by weak directed As–As bonded interactions. As observed for arsenic, the As–As bond paths for *claudetite* I connect the cap-shaped Lewis-base regions on As atoms on adjacent layers, forming directed bond paths generated by Lewis acid–base interactions. Professor Emil Makovicky at the University of Copenhagen (personal communication) not only believes that the interlayer bonded interactions in such layered molecular crystals are directional, but that all vdW interactions in a crystal structure are directional.

It is important to note that the intermolecular vdW interactions found for solid chlorine and arsenolite, for

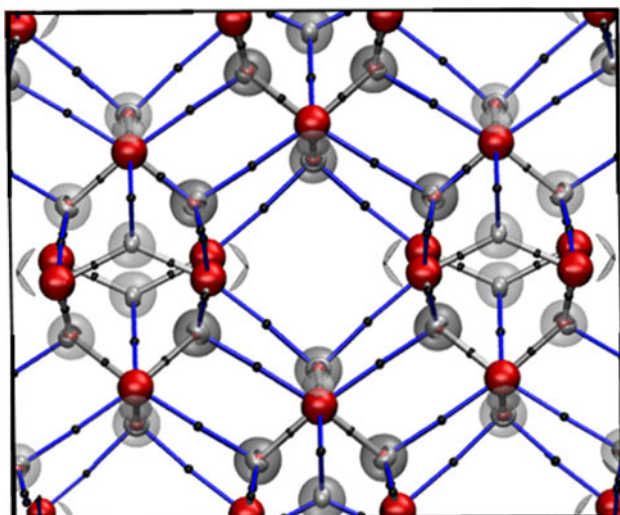


Fig. 6 $L(r)$ map for a representative moiety of the arsenolite structure viewed down [110] displaying the intermolecular As–O bond paths. Blue As–O bond paths connect the *red sphere* (Lewis-acid region) surrounding the nucleus of each As atom and the *silver ear muff-shaped* lone-pair (Lewis-base region) partly enclosing each O atom, qualifying as a Lewis acid–base interaction. The *ear muff-shaped envelope* capping each O atom on the reflex side of the As–O–As was calculated at the +12 a.u. level, and the *red sphere* enclosing the nucleus of each As was calculated at the –22 a.u. level. The *silver-colored skull cap-shaped envelope* on the As atom at the apex of each AsO_3 pyramid, calculated at the +0.01 a.u. level, defines a relatively low-lying Lewis-base lone-pair region. See Fig. 4 legend for further details

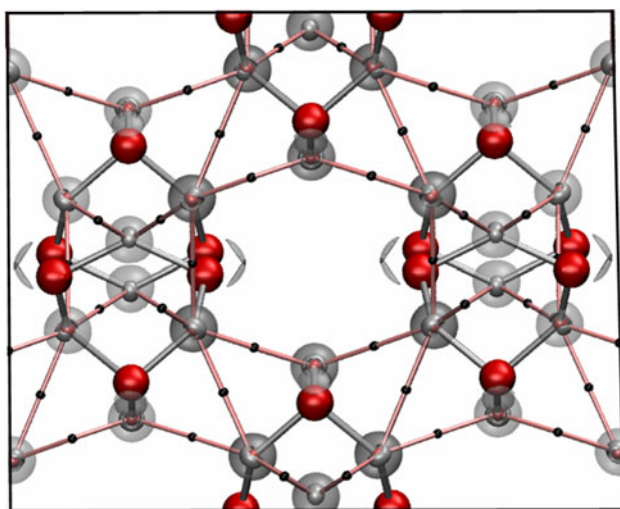


Fig. 7 $L(r)$ map for the arsenolite structure viewed down [110] displaying the O–O bond paths. The *pink lines* represent the intermolecular O–O bond paths that connect the *ear muff-shaped* lone-pair regions on the O atoms and define the Lewis base–base bonded interactions

example, are substantially different from the isotropic intermolecular interactions expected between gases and liquids endowed with interacting oscillating dipoles, fluctuating ED distributions and dispersion forces. Unlike these

interactions, the vdW interactions found for the two crystals are the result of long-range Lewis acid–base type interactions of the type found by Bader et al. (1984) where the approach of the reactants is determined by the alignment of the base and acid region on the adjacent reacting molecules. The intermolecular interactions in the two crystals and the others discussed above are concluded to belong to a new class of long-range Lewis acid–base intermolecular interactions, distinct from the traditional class of nondirectional vdW dispersion dipole–dipole interactions. The connection between the bond paths and the Lewis acid–base regions indicates that the structuralizing intermolecular forces of the vdW interactions in molecular crystals are encrypted in the $L(r)$ distribution. Although the molecules in the thioarsenides have been reported by earlier workers to be structuralized in terms of unspecified vdW nondirectional interactions, we will demonstrate that the structuralization of the molecules can also be understood in terms of long-range closed-shell Lewis acid–base type vdW interactions.

Thioarsenide molecular crystals

We have calculated and examined the ED distributions, the bond paths, the bond critical point properties, the local-energy density properties and $L(r)$ envelopes for seven nonequivalent thioarsenide molecular structures with the goal of establishing whether the bonded interactions that bind the molecules as crystals involve directed bond paths that connect Lewis acid–base regions similar to those observed for solid chlorine and arsenolite. The thioarsenides considered are the α - (realgar), β - and pararealgar AsS polymorphs, the As_4S_3 polymorphs α - and β -dimorphite, uzonite, As_4S_5 , and alacránite, As_8S_9 , each periodic structures that qualify as molecular inorganic crystals. The AsS polymorphs each consist of As_4S_4 molecules and α - and β -dimorphite both consist of As_4S_3 molecules, uzonite consists of As_4S_5 molecules and alacránite, As_8S_9 , consists of both As_4S_4 and As_4S_5 molecules in equal numbers [The thioarsenide nomenclature recommended by Bonazzi and Bindi (2008) is followed in this report].

In a recent examination of directed intermolecular and nonlocalized bonded interactions for organic molecules, Dunitz and Gavezzotti (2005) assert that topological studies of the type discussed above place too much emphasis on intermolecular cohesion involving pairs of atoms connected by directed bond paths and far too little on packing considerations. In contrast, in the case of the inorganic molecular materials examined in this study, it will be demonstrated that directed bonded interactions involving Lewis acid–base regions of ED and the Aufbau rule go hand-in-hand and together play an important role in

determining the structures of thioarsenides. Further, each of the thioarsenide molecular crystals examined in this study consist of close-packed molecules, suggesting that directed interactions and close packing also go hand-in-hand.

In a comprehensive tutorial paper on sulfide structures, Makovicky (2006) observed that it is often difficult to visualize the structuralization adopted by the molecules in a molecular thioarsenide crystal like realgar (no linkages are drawn that define the intermolecular bonded interactions; see Figure 44a in Makovicky 2006). On the other hand, as observed for arsenolite (Fig. 5), the mapping of the intermolecular bond paths has not only made it possible to generate the ED distribution associated with these features, but also to visualize, construct models and study the three-dimensional structuralization of the molecules. Indeed, knowledge of the intermolecular bond paths is expected to advance our understanding of the properties and the crystal chemistry of the thioarsenides. It may also be expected to reveal how the As_4S_4 and the As_4S_5 molecules in alacránite, As_8S_9 , are bonded and structuralized in space relative to one another. In addition, the paths and bonded interactions may shed light on why Se preferentially replaces a given sulfur atom in the realgar structure (Kyono 2009). It will also be of interest to explore the extent to which the intermolecular directed bonded interactions are involved in the realgar–pararealgar transition (Ballirano and Maras 2006; Bonazzi and Bindi 2008; Kyono et al. 2005; Naumov et al. 2007). The bond paths may be expected to provide a theoretical basis for the Makovicky and Mumme (1983) inverted lone pair micelle model (Moëlo et al. 2008) and the structuralizing of the As_4S_n ($n = 3, 4$ and 5) molecules by ‘weak vdW bonded interactions.’ Equally important, knowledge of the bonded interactions may be expected to advance the understanding of the diverse chemical behavior, transport and sequestration properties of the arsenic sulfides and oxides as toxins in the natural environment (Smedley and Kinniburgh 2002; Welch et al. 2000). In particular, a knowledge of the bond paths may also be expected to clarify the interactions that occur between water and the thioarsenides in a hydrothermal environment with the removal of As and the formation of such deadly toxins as arsine, AsH_3 , arsenite acid, $\text{As}(\text{OH})_3$ and arsenic acid, H_3AsO_4 (O’Day 2006).

Bond paths, the value of $\rho(\mathbf{r}_c)$ and the local-energy properties

As the bond paths and the structure of a material are determined by gradient vector field, $\nabla\rho(\mathbf{r})$, of the ED distribution, the ED was calculated for thioarsenides, and the bond paths were tracked using the elegant software

packages CRYSTAL98 (Saunders et al. 1998) and TOPOND (Gatti 1997). The 6-31d51G basis set for the arsenic atom (Towler et al. 1995) and the 86-311G* basis set for the sulfur atom (Lichanot et al. 1993) were especially optimized for our calculations. The bond critical points, \mathbf{r}_c , for the bonded interactions were found using an automated eigenvector-following search-algorithms performed on a region of space within a radius of 6 Å in diameter centered at each nonequivalent atom. Bond paths were not only found to exist for both the intramolecular As–S and As–As bonded interactions but also for intermolecular As–S, As–As and S–S bond interactions that structuralize the molecules in three-space. In each case, the paths were traced by mapping the gradient vector field of the ED distribution starting at \mathbf{r}_c and terminating at the nuclei of a pair of atoms connected by the bond path. As a bond path is intrinsically connected with a line of maximally negative potential energy density, Bader (1998) concluded that the presence of a bond path, together with its topologically equivalent virial path, serves as a universal indicator of a bonded interaction. Moreover, as the ED is topologically determined by the virial field, the presence of the virial path results in a line of maximum ED, a bond path and a state of electrostatic equilibrium between the pair. When these conditions are satisfied, the presence of a bond path suffices as evidence that a pair of atoms is bonded. Indeed, all atomic interactions that result in bond paths, including vdW interactions, are responsible for structuralizing the atoms in molecules and crystals (Bader 1998). In many cases, the greater the value of the ED at \mathbf{r}_c , denoted $\rho(\mathbf{r}_c)$, the stronger the bonded interaction and the shorter the bonded interaction.

Local-energy density properties

The kinetic density, $G(\mathbf{r})$ (a.u.) at a given point \mathbf{r} in a ground state material, can be related directly to the inner product of the gradients of the orbital electron densities ρ_i and their occupation numbers, n_i , by the expression

$$G(\mathbf{r}) = \frac{1}{8} \sum_i n_i [\nabla\rho_i(\mathbf{r}) \cdot \nabla\rho_i(\mathbf{r}) / \rho_i(\mathbf{r})],$$

where the summation is completed over the natural spin-orbital components (Parr and Yang 1989). With a determination of the positive definite local kinetic energy density, $G(\mathbf{r}_c)$, the negative definite local potential energy density, $V(\mathbf{r}_c)$, may be determined at the bond critical point, \mathbf{r}_c , if the Laplacian $\nabla^2\rho(\mathbf{r}_c)$ is known, using the local form of the virial theorem, $V(\mathbf{r}_c) = 1/4\nabla^2\rho(\mathbf{r}_c) - 2G(\mathbf{r}_c)$ (Bader 1990). The total local-energy density, defined as $H(\mathbf{r}_c) = G(\mathbf{r}_c) + V(\mathbf{r}_c)$ (Cremer and Kraka 1984), is asserted to be negative for shared interactions and positive for closed-shell

interactions. It has been argued that the sign of $H(\mathbf{r}_c)$ is determined by the energy density itself and therefore is negative for all interactions which result from an accumulation of ED at \mathbf{r}_c (see Bader 1990 for a comprehensive discussion of the topological properties and their use in evaluating the bonded interactions in materials).

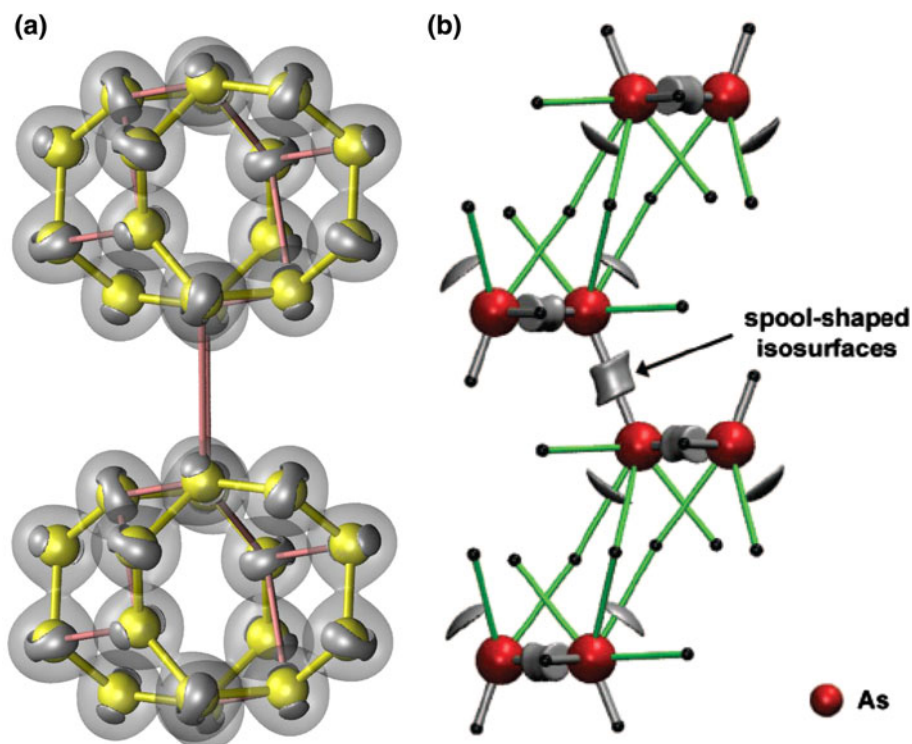
Properties of the ED distributions calculated for the thioarsenide molecules

The ED distributions were calculated, and bond paths were tracked for representative As_4S_n ($n = 3, 4$ and 5) molecules for the following seven thioarsenides: (1) alacránite As_8S_9 (Bonazzi et al. 2003); (2) uzonite, As_4S_5 (Bindi et al. 2003; Whitfield 1973a); (3), the low temperature realgar α -AsS polymorph (Kyono et al. 2005); (4) the high temperature β -AsS polymorph stable above $\sim 260^\circ\text{C}$ (Burns and Percival 2001) that slowly transforms upon cooling; (5) the AsS polymorph, pararealgar (Bonazzi et al. 1995); (6) the low temperature α -dimorphite As_4S_3 polymorph stable at room temperature (Whitfield 1970) and (7) the high temperature β -dimorphite polymorph stable above 130°C (Whitfield 1973b). Uzonite consists of a periodic array of neutral As_4S_5 molecules, the AsS polymorphs consist of neutral As_4S_4 molecules, the dimorphite polymorphs consist of neutral As_4S_3 molecules, and alacránite, unlike the other thioarsenides, consists of an ordered array of two nonequivalent neutral As_4S_4 and As_4S_5 molecules in equal

numbers. In each case, workers have asserted that the As and S atoms of the molecules are covalently bonded and that the molecules are structuralized as a crystal by an unspecified system of nondirectional vdW bonded interactions (Bindi et al. 2003; Bonazzi and Bindi 2008; Bonazzi et al. 1995, 2003; Burns and Percival 2001; Kyono et al. 2005; Makovicky 2006).

Each of the As_4S_n ($n = 3, 4$ and 5) molecule contains both As–S and As–As bonded interactions with the number of As–S and As–As intramolecular bonded interactions equaling $2n$ and $6 - n$, respectively. The three AsS polymorphs and alacránite each contain As_4S_4 molecules with eight As–S and two As–As bonded interactions. However, the molecules in pararealgar are different in that one of the As atoms is bonded to two As atoms and one S atom, two are bonded to one As and two S atoms, and one is bonded to three S atoms, whereas each As in the As_4S_4 molecule in the α - and β -polymorphs and alacránite are each bonded to one As atom and to two S. Further, as demonstrated below, the calculated $L(\mathbf{r})$ envelopes for the S and As atoms for the two molecules are comparable with those calculated for the S atoms comprising native sulfur and the As atoms comprising bulk native arsenic (Fig. 8a, b, respectively). The yellow envelope sphere (an Lewis-acid region) enclosing each S atom of the crown-shaped S_8 rings of sulfur in Fig. 8a was calculated at -0.1 a.u. level; the ear muff-shaped silver-colored Lewis base lone-pair envelope encircling much of each S atom was calculated at the $+1.25$ a.u. level. The silver-colored hourglass-shaped

Fig. 8 Moieties of the structures of **a** native sulfur viewed normal to (110) and **b** the bulk arsenic structure viewed down [010]. The S atoms and the S–S intramolecular bond paths are colored *yellow*, and the S–S intermolecular bond paths are colored *pink*. The *silver ear muff-shaped envelope* partly enclosing the S atoms was calculated at the $+1.25$ a.u., and the *hourglass-shaped envelope* was calculated at the $+0.001$ a.u. level. The *spool-shaped envelope* centering the As–As intramolecular bond paths and *cap-shaped envelope* located at the apex of the As_3 triangles were both calculated at the $+0.001$ a.u. level, and the *red spherical envelope* inclosing the nucleus of the As atom was calculated at the $+7.0$ a.u. level



envelopes enclosing the lone-pair envelopes on adjacent S atoms were calculated at the $+0.001$ a.u. level. The intramolecular bond paths that connect the S atoms of the eight-membered rings are colored yellow, whereas intermolecular bond paths that connect the rings together into a coherent structure are colored pink. The hourglass-shaped envelopes that narrow at the centers of each the intramolecular S–S bond path represent a localization of the ED along the bond path that connects the S atoms of the rings. The lengths of S–S bond paths in native sulfur range in value between 3.38 and 4.03 Å with an average value of 3.67 Å. The red spherical envelope enclosing each As atoms comprising bulk arsenic (Fig. 8b) was calculated at the -22.0 a.u. level; the spool-shaped envelopes centering the intramolecular As–As bond paths and the caps located at the apices of the As_3 triangles of the structure were both calculated at the $+0.001$ a.u. level. The spool-shaped envelope shows that ED is locally concentrated between the As atoms comprising the intramolecular As–As bonded interactions, while there is an absence of localized ED between the As atoms comprising the vdW intermolecular bonded interactions. Two of the three intermolecular bond paths branch from spherical-shaped acid surface on the As

atom and pass through the cap-shaped Lewis base envelopes, representing an acid and base directed bond paths associated with the weaker intermolecular As–As vdW interactions. The lengths of the intramolecular As–As bond paths range between 2.29 and 2.31 Å, while the lengths intermolecular As–As bond paths range between 3.53 and 3.85 Å with average value of 3.69 Å.

Pictures of the four topologically representative As_4S_n ($n = 3, 4$ and 5) molecules comprising the thioarsenides together with superimposed $L(r)$ envelopes for the molecules are displayed in Fig. 9. The geometry of each of the molecules displayed in the figure was optimized at the BLYP3/6-311G(2d, p) level. The As atoms are colored green, the S atoms are yellow, and the intramolecular bond paths between the atoms of the two molecules are silver. This color scheme for the atoms and the intramolecular bond paths will be used through out the remainder of the paper. Despite that each molecule has four As atoms and that the number of S atoms range between 3 and 5, the optimized As–S bond lengths for the molecules show little variation and range between 2.27 and 2.31 Å with an overall average value of 2.29 Å while the As–As bond lengths range between 2.53 and 2.57 Å with an average of

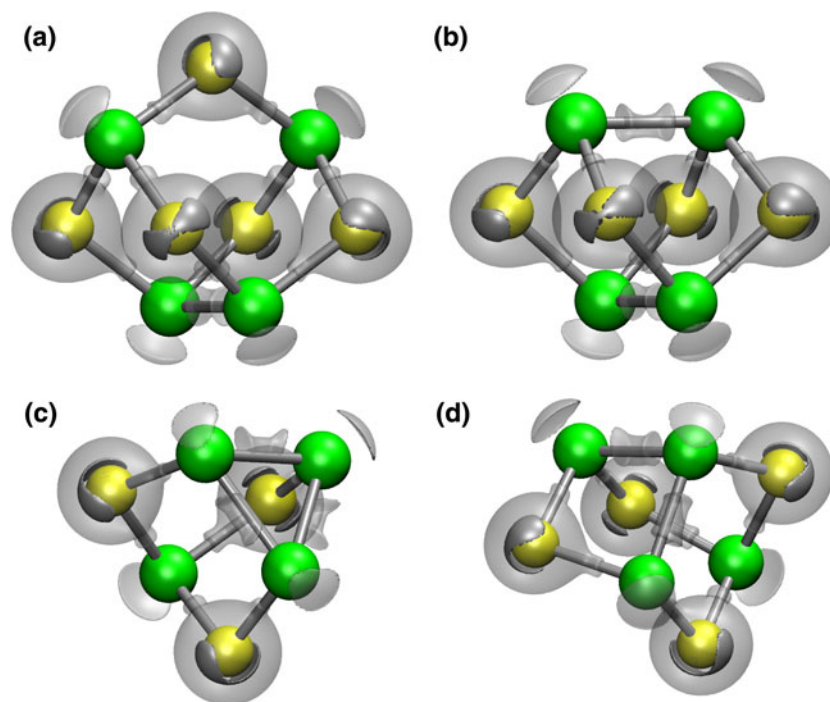


Fig. 9 Geometry optimized representative molecules observed for the thioarsenides. **a** The As_4S_5 molecule comprising the structures for uzonite and alacránite, As_8S_9 , **b** the As_4S_4 molecule comprising the structures of α - (realgar) and β -AsS and alacránite, **c** the As_4S_3 molecule comprising the structures of α - and β - dimorphite and **d** the As_4S_4 molecule comprising the structure of pararealgar. Envelopes of constant $L(r)$ values are superimposed on each of the molecules. The green spherical envelope (a Lewis-acid region) enclosing the nucleus

of each of the As atoms was calculated at the -7.0 a.u. level, the yellow sphere enclosing the nucleus of each S atom was calculated at the -0.1 a.u. level; the gray bulb-shaped envelope surrounding the S, the cap-shaped envelope associated with each As atom and the spool-shaped centering the As–As bond paths were each calculated at the $+0.001$ a.u. level, and the gray ear muff-shaped envelope (Lewis-base region) partly surrounding each S atom was calculated at the $+1.25$ a.u. level

2.56 Å, a value that is ~ 0.25 Å longer than the As–As bonded interaction in bulk arsenic. The average As–S bond lengths observed for the molecules in the crystals also show a small range of values between 2.21 and 2.25 Å with an average value of 2.23 Å. On the other hand, the observed As–As bond lengths show a wider range of values between 2.45 and 2.60 Å with an average value of 2.53 Å. It is noteworthy that the average As–S bond length for molecules in the crystals is ~ 0.05 Å longer than that calculated for the molecules shown in Fig. 8 while the average As–As bond length in the crystals is ~ 0.10 Å longer than that observed for the molecules.

The S atoms for each molecule shown in Fig. 9 are enclosed in part by ear muff-shaped lone-pair Lewis-base region envelope [$L(\mathbf{r}) = +1.25$ a.u.]. Each is also enclosed by a diffuse envelope [$L(\mathbf{r}) = 0.001$ a.u.] like those observed surrounding the S atoms in native sulfur where the envelope has the shape of half an hourglass that extends in the directions of the two-coordinating As atoms (Fig. 8a). The extension of the local concentration of the ED in the direction of the As atom is ascribed to the formation of a bonded interaction between As and S with the concentration of the ED located closer to the S and than to the As atom. The As atoms are each capped by skull cap-shaped lone pair regions [$L(\mathbf{r}) = 0.001$ a.u.] like those observed capping the As atoms in native bulk arsenic and arsenolite (Gibbs et al. 2009). Also the spool-shaped $L(\mathbf{r}) = 0.001$ a.u envelopes, displayed along the As–As bonded interactions, are similar to those observed for the intramolecular As–As bonded interactions in bulk arsenic (Fig. 8b). The spool-shaped envelope centered along the

As–As bond paths is ascribed to a concentration of ED that is localized along the bond path linking the As atoms. The similarity of the spool-shaped features along the As–As bond paths for the molecules and for those in arsenic indicates that the As–As bonded interactions in the molecules are comparable but somewhat weaker than the intramolecular As–As bonded interactions in the metalloid. Clearly, the ED is substantially more locally concentrated in the lone-pair region of the S atoms than it is in the region of the cap-shaped lone pair of the As atoms, a result that indicates the lone-pair features on the S atoms are better developed in As-bearing sulfides than those on the As atoms.

Bond paths and $L(\mathbf{r})$ envelopes generated for thioarsenide molecular crystals

Alacránite (As_8S_9)

Figure 10a is a drawing of an ordered planar array of As_4S_4 and As_4S_5 molecules for alacránite (Bonazzi et al. 2003) together with the intramolecular As–S and As–As bond paths that define the shared bonded interactions among the As and S atoms of the molecules. The bond paths that define the intermolecular bonded interactions and structuralize the molecules of the crystal are not displayed in the drawing. Their omission makes it relatively difficult to picture the role played by intermolecular forces that structuralize the molecules into a coherent periodic structure. But, as demonstrated earlier for arsenolite, the study

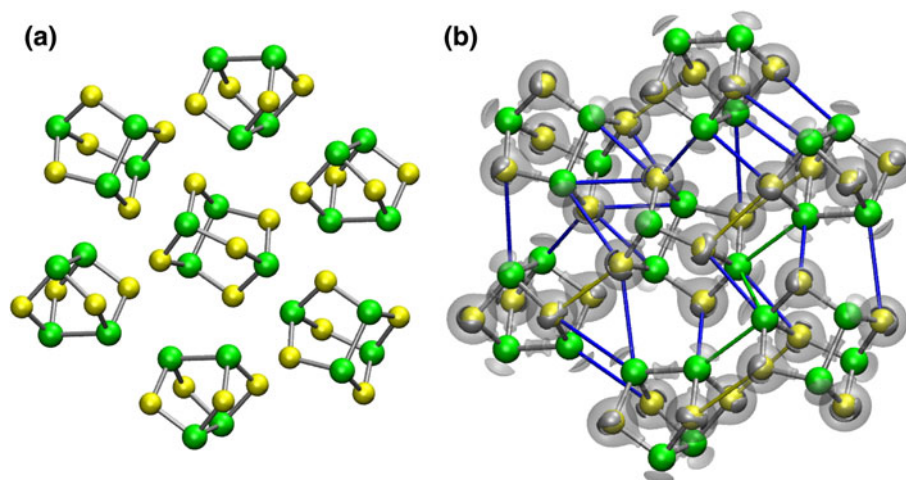


Fig. 10 **a** A moiety of the alacránite As_8S_9 structure. The *green spheres* represent As atoms and the *yellow* ones S atoms, connected by *silver* intramolecular bond paths. There are two types of molecules, As_4S_4 and As_4S_5 , such that each molecule is coordinated by 12 molecules in a distorted ccp array. The molecules in the moiety form a close-packed monolayer perpendicular to $[1\bar{1}1]$. **b** The moiety

displayed in **a** with the intermolecular bond paths that define the paths added to the moiety in **a**. The *blue lines* represent As–S paths, the *green* ones represent As–As paths, and the *yellow* ones represent S–S paths. $L(\mathbf{r})$ envelope maps are superimposed on the moiety [see Fig. 8 legend for the values of $L(\mathbf{r})$]. Note that the $L(\mathbf{r})$ -envelope maps are comparable to those displayed in Fig. 9

of molecular crystals in terms of both their intermolecular and intramolecular bond paths provides a new and important line of attack for studying and understanding the structure, properties and crystal chemistry of molecular crystals, particularly when crystal models of structures are constructed. Not only do the intermolecular bond paths provide a basis for picturing the spatial arrangement of the molecules, but when considered in conjunction with $L(\mathbf{r})$, they provide a basis for appreciating the role played by vdW bonded interactions in structuralizing the molecules.

The coordinates of the intermolecular and the intramolecular bond critical points are given in Table 1 for each of the thioarsenides including alacránite. With these coordinates and the coordinates of the atoms carefully determined for alacránite (Bonazzi et al. 2003), drawings and models

Table 1 Bond paths for alacránite (Bonazzi et al. 2003)

P (Å)	$\rho(\mathbf{r}_c)$ e/Å ³	x	y	z
As–S intramolecular bcp coordinates				
2.226	0.644	−0.0791	0.2704	−0.1000
2.227	0.643	0.0094	0.1539	−0.1524
2.206	0.663	−0.1731	0.3693	−0.2506
2.209	0.665	0.0845	0.4827	−0.1972
2.216	0.650	−0.4798	0.2458	0.4686
2.222	0.648	0.3646	0.2482	0.3777
2.239	0.623	0.4703	0.3793	0.3433
2.209	0.655	0.3854	0.0978	0.0877
2.238	0.625	0.3310	0.1010	0.2471
As–As intramolecular bcp coordinates				
2.582	0.432	0.0884	0.3182	−0.1077
2.568	0.436	0.5000	0.0371	0.2500
As–S intermolecular bcp coordinates				
3.557	0.069	0.0121	0.3294	0.0945
3.350	0.092	0.2772	0.2948	−0.0744
3.923	0.035	0.1514	0.2008	0.1316
3.628	0.060	0.1786	−0.4549	−0.0049
3.474	0.073	0.3146	0.3249	−0.4615
3.619	0.061	0.4662	0.4409	−0.4053
3.406	0.080	0.3901	−0.0664	0.3300
3.557	0.069	0.4896	−0.0631	0.0987
3.760	0.052	0.3327	−0.0680	0.0012
4.068	0.026	−0.0139	−0.0725	−0.1051
As–As intermolecular bcp coordinates				
3.691	0.058	0.3090	−0.4529	−0.1028
3.748	0.052	0.5000	−0.5000	−0.5000
S–S intermolecular bcp coordinates				
3.638	0.049	−0.1452	−0.0484	−0.2901
3.754	0.041	−0.1369	−0.3070	−0.2762
3.562	0.056	0.2466	0.2505	0.4858
3.812	0.039	−0.3354	−0.4399	0.3097

of the structure can be generated with the available software and examined. These drawings will show that the alacránite structure consists of a distorted cubic close-packed array of molecules that are interconnected by As–S, S–S and As–As intermolecular bond paths. They also show that the layer of molecules displayed in the Fig. 10a can be described as a distorted close-packed monolayer of molecules, paralleling approximately (11 $\bar{1}$). Each As₄S₄ molecule in the ccp array is coordinated by four As₄S₄ and eight As₄S₅ molecules while each As₄S₅ molecule is alternately coordinated by four As₄S₅ and eight As₄S₄ molecules. The distances between the barycenters of the two molecules in the cp array range between 6.18 and 7.55 Å with an average value of 6.89 Å. The distances between the barycenters for the As₄S₄ molecules range between 5.75 and 7.65 Å with an average value of 6.70 Å, whereas those between the As₄S₅ molecules range between 5.70 and 7.73 Å with an average 6.71 Å. The two different coordination sequences are ordered throughout the structure rather than being randomly distributed (Bonazzi et al. 2003), a result that may be expected given the directed nature of closed-shell As–S bonded interactions that structuralize the molecules into a crystal. The unique ordered array of As₄S₄ and As₄S₅ molecules results in the two molecules being segregated in alternate layers paralleling (100), the traces of which run diagonally from left to right shown in the Fig. 10a. It is notable that despite the different As/S ratios for the two molecules, the average separations between the barycenters of the As₄S₄ and the As₄S₅ molecules and their coordinating molecules are virtually the same.

The molecules displayed in Fig. 10b are copies of those displayed in Fig. 10a with the intermolecular As–S, As–As and S–S bond paths added (colored blue, green and yellow, respectively). This bond path coloring scheme will be used throughout the remainder of the paper. In addition, $L(\mathbf{r})$ envelopes are superimposed on the structure. The figure shows that the $L(\mathbf{r})$ maps for the intramolecular As–S and As–As bonded interactions for the As₄S₄ and As₄S₅ molecules are comparable with those displayed for the individual molecules (Fig. 9), a result that indicates that the local field of the molecules has little or no impact on the envelopes of the molecules. The bulk of the intermolecular As–S bond paths connect the acid regions of the As atoms of the molecules with the lone pair base regions of the S atoms on adjacent molecules, in effect corresponding to intermolecular Lewis base–acid-like chemical interactions. In addition, the intermolecular As–As bond paths that connect the As atoms on adjacent molecules are comparable with the intermolecular As–As bond paths displayed by bulk arsenic (Fig. 8b), and the intermolecular S–S bond paths are comparable with the intermolecular S–S bond paths displayed by native sulfur in Fig. 8a.

In particular, given that As–S bond paths connect the Lewis-acid regions on the As atoms and the Lewis-base regions on the S atoms, they qualify as long-range Lewis acid–base-directed bond paths. Collectively, these directed bond paths and the As–As and S–S paths are considered to serve as mainstays for the individual molecules that are repeated in the structuralization of a distorted periodic ccp array of molecules with parallel sets of directed bond paths. The As_4S_5 molecules in the structure are connected by V-shaped sets of As–S intermolecular bond paths while the As_4S_4 molecules are connected by parallel sets of As–S bond paths, features that will be found to be common in the other thioarsenites. In addition, parallel sets of intermolecular directed bond paths connect the Lewis-acid regions on the As and the Lewis-base regions of the O atoms in arsenolite (Fig. 4b). The intermolecular O–O bond paths in arsenolite that connect Lewis-base regions are comparable with the intermolecular S–S bond paths that connect Lewis-base regions in alacránite.

A total of 28 intermolecular bond paths branch out from each As_4S_4 molecule and 34 branches from each As_4S_5 molecule to the coordinating As_4S_4 and As_4S_5 molecules. Of those branching from each As_4S_4 molecule, 18 are As–S, 2 are As–As and 8 are S–S bond paths, whereas for those involving the As_4S_5 molecule, 24 are As–S, 2 are As–As and 8 are S–S paths. Of the bond paths that branch out from the As_4S_4 molecules, 3 As–S paths branch from As1, 2 As–S and an As–As path branch from As2, 2 As–S and 2 S–S paths branch from S1, S2 and S3, respectively. In the case of the As_4S_5 molecules, 3 As–S and an As–As path branch from As3, 3 As–S paths branch from As4, 2 As–S and 3 S–S paths branch from S4, 2 As–S and 2 S–S paths branch from S5 and 3 As–S paths branch from S6. There are a total of ten nonequivalent intermolecular As–S bond paths, four nonequivalent S–S bond paths and two nonequivalent As–As bond paths in alacránite (Table 2). The relatively large number of bond paths is directly related to the cheek-by-jowl close-packed array of the As_4S_4 and As_4S_5 molecules. The As–S bond paths range in length between 3.35 and 4.07 Å with the value of $\rho(\mathbf{r}_c)$ increasing linearly from 0.03 to 0.09 $\text{e}/\text{Å}^3$ with decreasing bond length. Given the accumulation of the ED along the bond path, the As–S bonded interactions are considered to result from the net electrostatic attraction exerted on the nuclei of the As and S atoms by the ED accumulated between the atoms (Feynman 1939). Of the As–S bond paths, the lengths of the three exceed the sum of the vdW radii for As and S [$R_{\text{vdW}}(\text{As–S}) = 1.85 + 1.80 \text{ Å} = 3.65 \text{ Å}$]. The vdW radii are used as a matter of convenience as a means of gauging the relative strengths of the intermolecular bonded interactions. The seven bond paths that are less than $R_{\text{vdW}}(\text{As–S})$ range between 3.35 and 3.63 Å with an average value of 3.51 Å. On the basis of these values, the As and S atoms of

Table 2 Bond paths for uzonite (Bindi et al. 2003)

P (Å)	$\rho(\mathbf{r}_c)$ $\text{e}/\text{Å}^3$	x	y	z
As–S intramolecular bcp coordinates				
2.241	0.622	0.1014	0.3536	−0.1454
2.262	0.600	0.4620	0.3715	−0.2352
2.251	0.616	0.3119	0.4746	−0.3962
2.237	0.632	0.2907	0.4760	−0.1757
2.250	0.613	0.1374	0.3521	0.4566
As–As intramolecular bcp coordinates				
2.530	0.458	0.0421	0.2500	−0.3676
As–S intermolecular bcp coordinates				
3.796	0.042	−0.2202	0.2500	−0.2044
3.654	0.054	−0.0804	0.1092	−0.0517
3.361	0.090	−0.1011	0.1144	−0.3322
3.361	0.098	−0.0869	0.1115	−0.4997
3.724	0.056	−0.0694	0.1070	0.2794
3.584	0.064	−0.4190	−0.4796	−0.3490
3.787	0.046	−0.3998	−0.4859	−0.0793
As–As intermolecular bcp coordinates				
3.734	0.048	0.5000	0.5000	0.0000
S–S intermolecular bcp coordinates				
3.452	0.063	0.0000	0.5000	0.0000
3.577	0.055	0.3211	−0.3922	0.0617
3.588	0.057	0.3464	−0.3943	0.3337

the molecules are indicated to mutually penetrate one another between 0.03 and 0.30 Å, the greater the penetration, the greater the value of $\rho(\mathbf{r}_c)$. As documented in a comprehensive study of hydrogen-bonded systems (Carroll and Bader 1988), such penetrations represent nontrivial bonded interactions, the greater the penetration, the greater the value of $\rho(\mathbf{r}_c)$ and the strength of the interaction. The four nonequivalent S–S bond paths range in length between 3.56 and 3.81 Å with an average value of 3.69 Å. Only one of the S–S bond paths has a length (3.56 Å) less the radius sum for the two S atoms, $3.60 \text{ Å} = R_{\text{vdW}}(\text{S–S})$, indicating that the S atoms mutually penetrate one another in a substantially smaller amount. The bond path lengths of the S–S interactions show a wider range of values in native sulfur, but the average value, 3.67 Å, is comparable with that observed for alacránite. Like the As–S bonded interactions, the $\rho(\mathbf{r}_c)$ values for the S–S interactions decrease regularly from 0.06 to 0.04 $\text{e}/\text{Å}^3$ with the decreasing separation between the S atoms. Of the two nonequivalent As–As bond paths, the length of one (3.75 Å) exceeds the additive sum of the radii for two As atoms, $R_{\text{vdW}}(\text{As–As}) = 3.70 \text{ Å}$ while the shorter one, 3.69 Å, is slightly less. As expected, the $\rho(\mathbf{r}_c)$ value for the shorter one, 0.06 $\text{e}/\text{Å}^3$, slightly exceeds that of the longer, 0.05 $\text{e}/\text{Å}^3$. The lengths of the intermolecular As–As bond paths range in value between 3.53 and 3.84 Å in bulk arsenic with an average value of 3.69 Å,

values that are comparable with those observed for alacránite. As expected, the mutual penetration of As by As and S by S on adjacent molecules is substantially less than the mutual penetration of As atoms and S atoms. The greater mutual penetration of the As and S atoms indicates that Lewis acid–Lewis lone-pair base As–S bonded interactions are typically stronger in governing the arrangement of the molecules in alacránite than As–As Lewis acid–acid and S–S Lewis base–base bonded interactions. The ordered patterns of the As_4S_4 and As_4S_5 molecules in the structure are considered to be, in large part, a result of the directed nature of the acid–base As–S bonded interactions, particularly given their larger numbers and greater mutual penetrations.

Uzonite (As_4S_5)

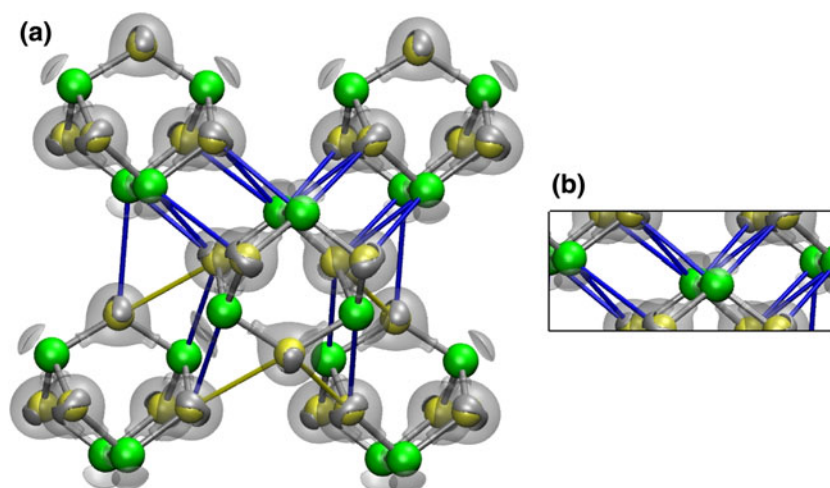
As we have seen, the structure of alacránite consists of a relatively complicated ordered array of ccp As_4S_4 and As_4S_5 molecules. In contrast, the structure of uzonite consists only of As_4S_5 molecules while the structures of the AsS polymorphs consist only of As_4S_4 molecules (Bindi et al. 2003; Whitfield 1973a). An examination of the molecules in uzonite and their associated intermolecular bond paths shows that As_4S_5 molecules are likewise arranged in a distorted ccp cheek-by-jowl array of molecules where each As_4S_5 molecule in the structure is coordinated by 12 As_4S_5 molecules. The distances between the barycenters of the molecules in uzonite show the largest range of values observed for the thioarsenides, ranging between 5.63 and 7.97 Å with an average separation of 7.02 Å. A representative moiety of the uzonite structure, viewed roughly parallel to the ^{1010}m mirror plane down [001], is displayed in Fig. 11a, where the molecules are bonded together in zigzag strings of As–S intermolecular

bond paths running perpendicular to the plane as described by Bindi et al. (2003).

As observed for alacránite, the $L(\mathbf{r})$ envelope maps for uzonite show that the features for the individual molecules are in close agreement with those displayed for the As_4S_5 molecules shown in Fig. 9 and for alacránite. It is evident from the figure that the As_4S_5 molecules are linked by a Z-shaped sets of directed bond paths, like those in alacránite, that branch from Lewis-base regions on the S atoms of the molecules to Lewis-acid regions on the As atoms of the adjacent molecules [see insert (b) in Fig. 11]. It is notable that Z-shaped sets of directed bond paths also connect the Lewis-base regions of the O atoms in arsenolite (Fig. 4a) as well as the Lewis-base regions of the O atoms and the Lewis-acid regions of the Sb atoms in sénarmonite, Sb (Whitten et al. 2004). The molecules in uzonite are also connected by S–S bond paths similar to intermolecular bonded interactions that bind the S_8 rings in native sulfur together into a coherent structure, along with one non-equivalent As–As bond path (not shown).

A total of 38 intermolecular bond paths branch out from each As_4S_5 molecule in uzonite to the 12 nearest-neighbor equivalent molecules of the cp array of molecules. Of these, 26 represent As–S, 10 S–S and 2 As–As bonded interactions. Five As–S bond paths branch from As1 and four from As2. Two As–S and an As–As bond paths branch from As3, 2 S–S and 3 As–S paths branch from S1, 3 As–S and a S–S paths branch from S2 and 1 As–S and 4 S–S paths branch from S3. The intermolecular As–S bond path lengths show a smaller range of values (3.36–3.80 Å) than observed for alacránite with three of the eight nonequivalent lengths being less than), ranging between 3.36 (2×) and 3.58 Å (Table 2). Each of the three nonequivalent intermolecular S–S bond lengths is less than $R_{\text{vdW}}(\text{S–S})$, ranging between 3.45 and 3.59 Å. The one nonequivalent

Fig. 11 **a** A moiety of the uzonite As_4S_5 structure with superimposed $L(\mathbf{r})$ envelopes and **b** an insert displaying the Z-shaped sets of As–S bond paths. See Fig. 9 legend for atom nomenclature and Fig. 10 for bond path definitions and the values of $L(\mathbf{r})$



As–As bond path length, 3.73 Å, exceeds $R_{vdW}(As-As)$. As observed for alacránite, the intermolecular As–S and S–S bond path lengths decrease linearly with decreasing $\rho(\mathbf{r}_c)$. The mutual penetrations of the As and S atoms range between 0.06 and 0.29 Å while the mutual penetration of the S atoms ranges between 0.01 and 0.15 Å. The ordering of the molecules in uzonite as a distorted ccp array can be ascribed to Z-shaped sets of directed As–S bond paths and parallel sets of directed S–S bond paths. As observed for alacránite, the $L(\mathbf{r})$ envelopes for S–S and As–As bonded interactions are comparable with those displayed for native S and arsenic, respectively. The 38 intermolecular bond paths that branch out from each As_4S_5 molecule in uzonite is larger than that observed for the As_4S_5 molecule in alacránite (Bonazzi et al. 2003). It is also larger than that observed for the smaller As_4S_4 molecules in alacránite as well as that observed for the smaller As_4S_4 molecules in realgar (Ballirano and Maras 2006), pararealgar (Bonazzi et al. 1995) and α -AsS (Burns and Percival 2001), indicating that the number of potential bond paths that branch from a As_4S_n molecule is related to the size of the molecule, not surprising, the larger the molecule and the greater the number of S atoms, the greater the number of branching bond paths.

α -AsS (realgar) and β -AsS

In a careful study of the structure of realgar, Ito et al. (1952) asserted that potential intermolecular bonded interactions with lengths less than 4.0 Å contribute to the cohesion of the molecules while those greater than 4.0 Å do not. In agreement with this assertion, of the 11 nonequivalent intermolecular As–S bond paths calculated for realgar, all were found to be less than 4.0 Å, ranging between 3.42 and 3.84 Å (Table 3). Of the 11, seven are less than 3.65 Å with an average value of 3.52 Å. An examination of the arrangement of the molecules in realgar (Kyono et al. 2005) together with the calculated bond paths shows that molecules are structuralized in a very highly distorted ccp array with the cp monolayers paralleling (100). The average distances between the barycenters is 6.76 Å with the distances ranging in value from 5.17 to 8.54 Å. A total of 31 intermolecular bond paths branch out from each As_4S_4 molecule, connecting the adjacent 11 nearest-neighbor molecules. Of these, 23 represent As–S, 6 As–As and 2 S–S bonded interactions. Three As–S and 2 As–As paths branch from As1, 4 As–S and an As–As path branches out from As2, 3 As–S and an As–As branches from As3, and 2 As–S and 2 As–As paths branches from As4, 3 As–S and an S–S path branches from both S1 and S2, 3 As–S paths branch from S3 and 2 As–S paths branch from S4.

Figure 12 is a representative moiety of the structure viewed roughly perpendicular to (5 2 $\bar{1}$). The molecules in

Table 3 Bond paths for realgar (Kyono et al. 2005)

Unit cell						
<i>a</i> (Å)	<i>b</i> (Å)	<i>c</i> (Å)	β	S.G.		
6.590	13.563	9.770	113.811	P2 ₁ /c		
Atomic coordinates						
Atom	<i>x</i>	<i>y</i>	<i>z</i>			
As1	−0.6424	−0.0206	0.1211			
As2	−0.4322	0.1388	0.4240			
As3	0.1428	0.1264	0.3208			
As4	−0.6752	0.1609	0.0395			
S1	−0.3567	−0.0064	0.3440			
S2	0.0991	−0.0234	0.2138			
S3	−0.4013	0.2261	0.2380			
S4	0.0549	0.2103	0.1071			
Bond path length, <i>P</i> and bcp coordinates						
	<i>P</i> (Å)	$\rho(\mathbf{r}_c)$ e/Å ³	<i>x</i>	<i>y</i>	<i>z</i>	
Intramolecular bond paths						
As–S	2.230	0.641	0.2340	−0.0207	0.1671	
	2.241	0.629	0.4938	−0.0127	0.2292	
	2.247	0.623	−0.4193	0.1799	0.3328	
	2.248	0.622	−0.3980	0.0690	0.3833	
	2.231	0.639	0.4558	0.1917	0.1367	
	2.240	0.629	0.1022	0.1661	0.2171	
	2.250	0.618	0.1234	0.0547	0.2682	
	2.236	0.660	0.1960	0.1841	0.0743	
	As–As	2.573	0.436	0.3553	0.1311	0.3663
		2.572	0.437	0.3415	0.0713	0.0861
Intermolecular bond paths						
As–S	3.490	0.077	0.1375	0.0010	−0.0421	
	3.671	0.056	0.3893	−0.1469	0.1924	
	3.510	0.068	−0.4159	0.2075	−0.4146	
	3.585	0.068	0.4615	0.0757	−0.4638	
	3.614	0.059	−0.1873	0.2150	−0.4815	
	3.417	0.079	0.2580	0.0716	0.4896	
	3.606	0.066	−0.1302	0.1731	0.2806	
	3.444	0.077	0.1236	0.0880	−0.0817	
	3.842	0.044	−0.1136	0.0645	0.3261	
	3.680	0.057	0.2728	−0.0827	0.3949	
	3.755	0.052	−0.1537	0.1125	−0.0059	
	As–As	3.622	0.062	−0.4815	−0.0920	0.0395
		3.563	0.069	0.4412	0.2345	0.4806
3.503		0.078	0.2366	0.2300	0.4288	
S–S	3.610	0.060	0.5000	0.0000	0.0000	
	3.716	0.044	−0.1259	−0.0098	0.2740	

the figure are linked together by As–S and As–As intramolecular bonded interactions. Like the As–S intermolecular bonded interactions in both alacránite and uzonite, the bond

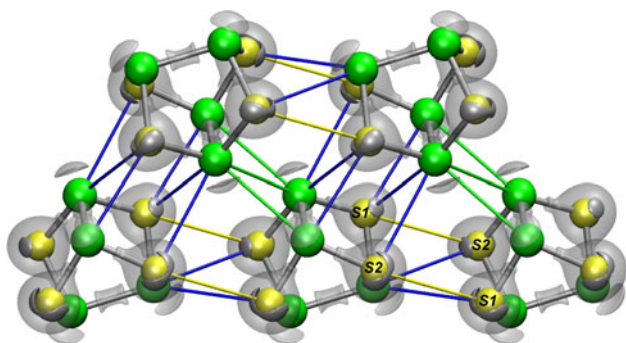


Fig. 12 A moiety of the structure of the realgar α -AsS polymorph viewed down approximately $[52\bar{1}]$ with $L(\mathbf{r})$ envelopes. See Figs. 9 and 10 for details

paths connect the acid regions on the As atoms with the base regions on the S atoms in Z-shaped sets of bond paths. Likewise, the As–As intermolecular interactions are virtually the same as those observed for arsenic, also adopting a Z-shaped set of bond paths. There exists one nonequivalent S–S bond path that connects the S1 atom and S2 atoms on adjacent molecules at a distance of 3.71 Å. A parallel set of S1–S2 bond paths are labeled in Fig. 12. In a careful study of the substitution of S in realgar by Se, Kyono (2009) demonstrated that Se has a strong tendency to replace both S1 and S2 as discussed below. The intermolecular S–S bond paths connect the Lewis-base regions on one molecule and a Lewis-acid regions on adjacent molecule forming a long-range Lewis acid–base bonded vdW interaction.

Of the 11 nonequivalent As–S intermolecular bond paths, seven are less than $R_{\text{vdW}}(\text{As–S})$ with bond lengths ranging between 3.42 and 3.61 Å with an average value of 3.52 Å while the remaining longer four range between 3.68 and 3.84 Å. The mutual penetrations of the As and S atoms on adjacent molecules in realgar is comparable with those observed for alacránite and uzonite. Of the four nonequivalent As–As bond paths, all of the associated bond lengths are less than 3.70 Å, ranging between 3.50 and 3.62 Å with an average value of 3.57 Å. In contrast, the mutual penetration of the As atoms on adjacent molecules is substantially greater than that observed for alacránite, ranging between 0.08 and 0.20 Å. As the length of the S1–S2 path, 3.71 Å, is substantially longer than $R_{\text{vdW}}(\text{S–S})$, the S1–S2 interaction is indicated to be relatively weak.

As the As_4S_4 molecule in the high temperature β -AsS polymorph (Burns and Percival 2001) has the same topology as the molecule in realgar, the bond path and $L(\mathbf{r})$ properties of the polymorph are considered here for comparison (Fig. 13). Unlike realgar, each of the As_4S_4 molecules in β -AsS is coordinated by 12 equivalent molecules arranged in a distorted ccp array with the separations between the barycenters of the molecules ranging between 5.77 and 7.40 Å with an average separation of 6.68 Å. Unlike realgar, β -AsS

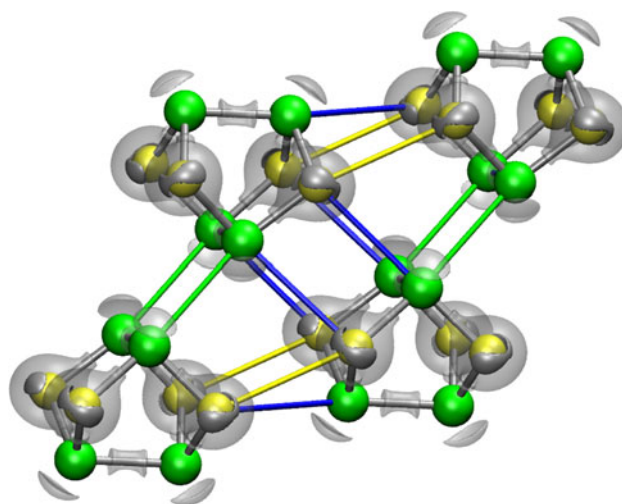


Fig. 13 A moiety of the structure of the β -AsS polymorph viewed down approximately $[11\bar{1}]$ with superimposed $L(\mathbf{r})$ envelopes. See Figs. 9 and 10 legends for details

contains strings of S–S intermolecular bond paths that extend uninterrupted throughout the structure paralleling $[101]$. As observed for the other thioarsenide materials, the features of $L(\mathbf{r})$ envelope maps for the S–S and As–As intermolecular interactions are comparable with those displayed by native sulfur and arsenic. Rather than being connected by a Z-shaped configuration of As–S bond paths, the molecules in β -AsS are connected by parallel sets of As–S bond paths as observed between the As_4S_5 molecules in alacránite. A total of 28 intermolecular bond paths branch out from each As_4S_4 molecule in β -AsS connecting to the 12 coordinating As_4S_4 molecules: 18 are As–S, 4 are As–As and 6 are S–S bond paths. 2 As–S and 1 As–As paths branch from both As1 and As2, 4 As–S paths branches from S1 and 3 S–S and 1 As–S path branches from S2. The lengths of the nonequivalent As–S bond paths are 3.54, 3.67 and 3.72 Å, only one of which is less than $R_{\text{vdW}}(\text{As–S})$ (Table 4). Of the three nonequivalent S–S bond paths of length (3.35, 3.74 and 3.74 Å), only one is less than $R_{\text{vdW}}(\text{S–S})$. Like realgar, sets of parallel S–S bond paths connect the As_4S_4 molecules. The one nonequivalent As–As bonded interaction is 0.12 Å shorter than $R_{\text{vdW}}(\text{As–As})$. On the basis of these results, it is apparent that the intermolecular bonded interactions in β -AsS are not as well developed and as strong as those in realgar. The widespread occurrence of realgar in nature relative to that of the other AsS polymorphs (Bonazzi and Bindi 2008) may be ascribed to the larger number and the greater penetrations of As–S bonded interactions in realgar.

Pararealgar (AsS)

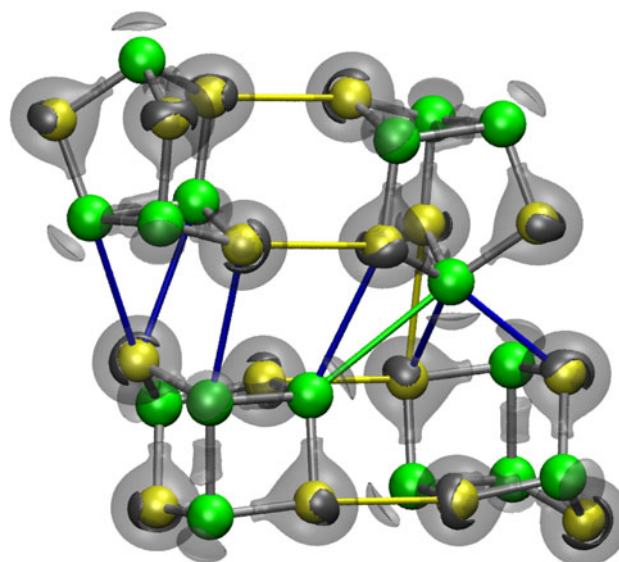
As observed above, realgar transforms into pararealgar when exposed to a beam of light at room temperature.

Table 4 Bond paths for β -AsS (Burns and Percival 2001)

P (Å)	$\rho(\mathbf{r}_c)$ e/Å ³	x	y	z
As–S intramolecular bcp coordinates				
2.225	0.644	0.0004	0.1352	0.1514
2.232	0.637	0.0970	0.2538	0.1087
2.229	0.642	0.4184	−0.0267	0.1882
2.216	0.654	0.1780	0.3548	0.2693
As–As intramolecular bcp coordinates				
2.599	0.422	−0.0763	0.3040	0.0984
As–S intermolecular bcp coordinates				
3.545	0.064	−0.0056	0.3241	−0.0967
3.668	0.054	−0.0018	0.0736	−0.1051
3.725	0.053	0.3171	0.0449	−0.0175
As–As intermolecular bcp coordinates				
3.588	0.064	−0.1661	0.1477	−0.0365
S–S intermolecular bcp coordinates				
3.740	0.043	−0.1556	−0.0667	0.2007
3.354	0.074	0.2500	0.2500	0.0000
3.740	0.043	0.3522	0.1744	0.2115

Furthermore, as observed, the As_4S_4 molecules in realgar and pararealgar are geometrical isomers in that one of the As atoms in the molecule for pararealgar (Bonazzi et al. 1995) is bonded to two As atoms and one S atom: two others are bonded to one As and two S atoms and one is bonded to three S atoms, whereas each As atom in the molecule in realgar is bonded to an As and to two S atoms. As observed for the molecules in β -AsS, each molecule in pararealgar is coordinated by 12 equivalent molecules in a distorted ccp array. The range of the separations (5.52 and 7.19 Å) between the barycenters of the molecules is smaller than that observed for alacránite and uzonite with an average value of 6.65 Å. As observed for alacránite, the close-packed layers for the two structures parallel (111). The intramolecular bond paths and the constant $L(\mathbf{r})$ value envelopes for the As and S atoms of the molecule in the pararealgar structure (Fig. 14) are virtually the same as those displayed for the molecule in Fig. 9d.

A total 29 bond paths branch out from each molecule in pararealgar to adjacent molecules (two fewer than observed for realgar) of which 21 represent As–S (two fewer than observed for realgar), 4 As–As and 4 S–S bonded interactions. Three As–S and 1 As–As paths branch from As1, 3 As–S and 1 As–As branch from As2, 2 As–S and 1 As–As branch from As3, 3 As–S and 1 As–As branch from As4, 2 As–S and 1 S–S branch from S1, 3 As–S and 2 S–S branch from S2, 2 As–S and 1 S–S branch from S3 and 3 As–S bond paths branch from S4. Of the ten nonequivalent intermolecular bond paths, five have bond lengths less than $R_{\text{vdW}}(\text{As–S})$ and range between 3.38 and 3.62 Å with an average value of 3.54 Å. The intermolecular As–As bond

**Fig. 14** A moiety of the structure of pararealgar, AsS, viewed down approximately $[1\bar{1}0]$ with superimposed $L(\mathbf{r})$ envelopes. See Figs. 9 and 10 legends for details

paths range in length between 3.66 and 3.80 Å, and the lengths of S–S bond paths range between 3.35 and 3.48 Å, comparable with the values observed for β -AsS, for example. The $L(\mathbf{r})$ envelope maps indicate that the As–S bonded interactions involve the Lewis-base region on the S atom and a Lewis acid on the As atoms as observed for other intermolecular As–S bonded interactions. Again, the envelopes for the intermolecular S–S and the As–As bonded interactions are comparable with those observed for native sulfur and bulk arsenic, respectively.

Given that a beam of light transforms realgar to pararealgar, the net charges for the two were calculated to determine the extent to which the charges conferred on the As and S atoms for the two polymorphs agree. The net charges were obtained by integrating $\rho(\mathbf{r})$ over the basins of the nonequivalent As and S atoms and then subtracting this average number of electrons from the nuclear charges of the two atoms. The net charges conferred on the As atoms [$q(\text{As}1) = 0.43$ e; $q(\text{As}2) = 0.44$ e; $q(\text{As}3) = 0.43$ e; $q(\text{As}4) = 0.38$ e] and the S atoms ($q(\text{S}1) = -0.43$ e; $q(\text{S}2) = -0.43$ e; $q(\text{S}3) = -0.43$ e; $q(\text{S}4) = -0.41$ e] in realgar are relatively small in magnitude and uniform in value. In contrast, the charges on the As atoms [$q(\text{As}1) = 0.66$ e; $q(\text{As}2) = 0.44$ e; $q(\text{As}3) = 0.44$ e; $q(\text{As}4) = 0.25$ e] and the S atoms ($q(\text{S}1) = -0.49$ e; $q(\text{S}2) = -0.45$ e; $q(\text{S}3) = -0.46$ e; $q(\text{S}4) = -0.43$ e] conferred on the atoms of pararealgar are less uniform in value and show a wider range of values. The $\text{As}1^{+0.66}$ atom with the largest net charge is bonded to three S atoms with intermediate charges ($\text{S}1^{-0.49}$, $\text{S}2^{-0.45}$ and $\text{S}4^{-0.43}$), and $\text{As}4^{+0.25}$ with the smallest net charge is bonded to $\text{As}2^{+0.44}$,

and $\text{As3}^{+0.44}$ and $\text{S4}^{-0.42}$ also with intermediate charges. The two remaining As atoms, $\text{As2}^{+0.44}$ and $\text{As3}^{+0.44}$, have intermediate net charges and are bonded to two S atoms and an As atom, $\text{S1}^{-0.49}$, $\text{S2}^{-0.45}$, $\text{As4}^{+0.25}$ and $\text{S2}^{-0.45}$, $\text{S3}^{-0.46}$ and $\text{As4}^{+0.25}$, respectively. The relatively wide range in the net charges conferred on the As and S atoms of the As_4S_4 molecule for pararealgar may be expected given the greater distortion and the asymmetric distribution of the As and S atoms in the molecule compared with the more uniform charges conferred on the molecule in realgar.

In a detailed study of the substitution of Se for S in realgar, Kyono (2009) documented that Se has a strong preference for replacing the S2 and S1 atoms of the As_4S_4 molecule, whereas it has an extremely weak preference to replace S3 and S4. The uniform net charges conferred on the S atoms for realgar provide little or no insight into the preferential replacement of S1 and S2 by Se. The charges calculated for the molecules using density functional theory (Bullen et al. 2003), while smaller in magnitude, likewise show little variation. Kyono (2009) concluded on the basis of the small variation in the DFT charges that the observed preferential replacement of S1 and S2 by Se is unrelated to the charges on the atoms. Like S2 and S1, the S3 and S4 atoms are both involved in two and three As–S intermolecular bonded interactions, respectively. But unlike S3 and S4, both S1 and S2, in addition to being bonded to As, are also bonded to S2 and S1, respectively. Together, they comprise a common S–S bond path between adjacent molecules (Fig. 14). Hence, the replacement of either of these S atoms by Se is expected to have virtually the same impact on both S atoms, providing a basis for why the preference of Se for either S1 or S2 is virtually the same. The relative weak nature of the S1–S2 bonded interaction may also contribute to the ease with which the bonded interaction is ruptured with the replacement S replaced Se. Like both realgar and $\beta\text{-As}_4\text{S}_4$, the molecules in pararealgar are connected by sets of parallel S–S bond paths.

α - and β -Dimorphite

Both of these supramolecules are orthorhombic with the same space group type, $Pnma$, and consist of As_4S_3 molecules. The As_4S_3 molecules in both α - and β -dimorphite are arranged in a distorted hcp array with the array in β -dimorphite being the more distorted of the two (Whitfield 1970). The cp monolayers parallel (010) in α -dimorphite and (100) in β -dimorphite (Whitfield 1973b). The average distance between the barycenters for the 12 coordinating molecules in α -dimorphite is 6.53 Å with a range of values between 5.22 and 7.19 Å, whereas the average distance is 6.83 Å in β -dimorphite with a range of values between 5.53 and 8.27 Å. Unlike the known thioarsenides, α -dimorphite is the only one that lacks S–S and As–As intermolecular

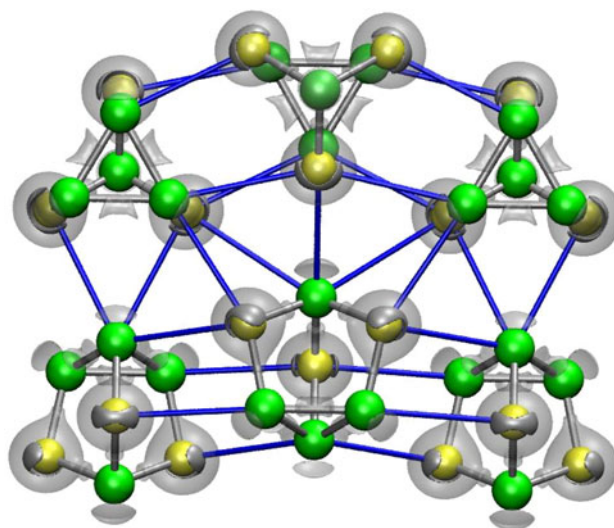


Fig. 15 A moiety of the structure of α -dimorphite, As_4S_3 , viewed along the symmetry plane of the ^{1010}m isometry. See legends of Figs. 9 and 10 for details

bond paths, only containing As–S intermolecular bond paths (Fig. 15). A total of 26 intermolecular As–S bond paths branch out from each molecule α -dimorphite with 3 branching from As1, 4 from As2, 3 from As3, 4 from S1 and 5 from S2. The lengths of intermolecular As–S bond paths all exceed $R_{\text{vdW}}(\text{As–S})$ except one with a length of 3.47 Å. The molecules are aligned in the structure in a key–lock fashion associated with parallel directed As–S bond paths that connect the acid regions of the As atoms and the lone pair base regions of the S atoms. In contrast, a total of 32 intermolecular bond paths branch out from each molecule in β -dimorphite of which 20 are As–S bond paths, 8 are S–S bond paths and 4 are As–As bond paths. A total of 5 branches from As1 consisting of 3 As–S and 2 As–As paths, a total of 4 branches from As2 of which all 4 are As–S paths and 4 branch from As3 of which 3 are As–S and 1 is an As–As bond path. There are five nonequivalent intermolecular As–S bond paths, two As–As and two S–S bond paths in β -dimorphite (Fig. 16). The lengths of the As–S and As–As bond paths show a relatively wide range of values between 3.53 and 4.07 Å, and 3.59 and 3.95 Å, respectively (Table 6). Like α -dimorphite, the molecules are aligned in a key–lock fashion by parallel directed As–S bonded interactions. In sharp contrast, the As atoms of molecules in β -dimorphite are connected by intermolecular As–As bond paths that form strings of alternating intermolecular and intramolecular As–As bond paths that continue uninterrupted parallel to [100] throughout the crystal (Fig. 17). There are five nonequivalent As–S intermolecular bond paths ranging in length between 3.53 and 4.07 Å with only one less than $R_{\text{vdW}}(\text{As–S})$. The two nonequivalent intermolecular As–As bond path lengths are 3.58 and 3.95 Å, and the two nonequivalent intermolecular S–S bond

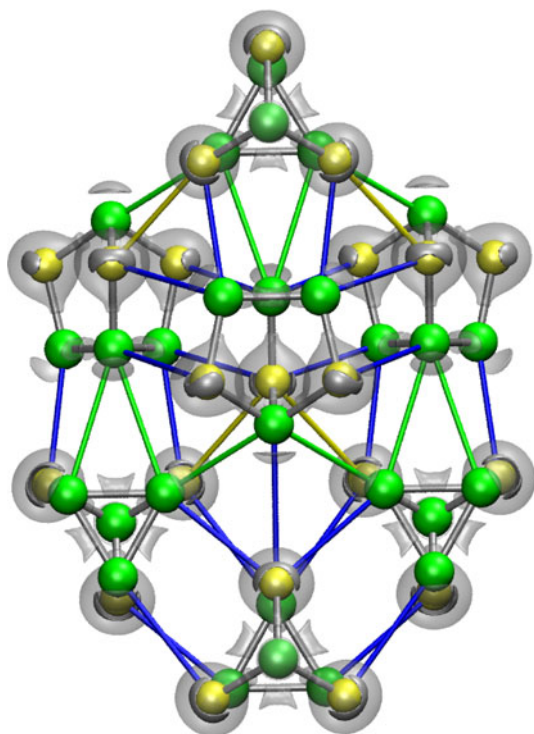


Fig. 16 A moiety of the structure of β -dimorphite, As_4S_3 , viewed along the symmetry plane of ^{1010}m isometry. For details, see legends of Figs. 9 and 10

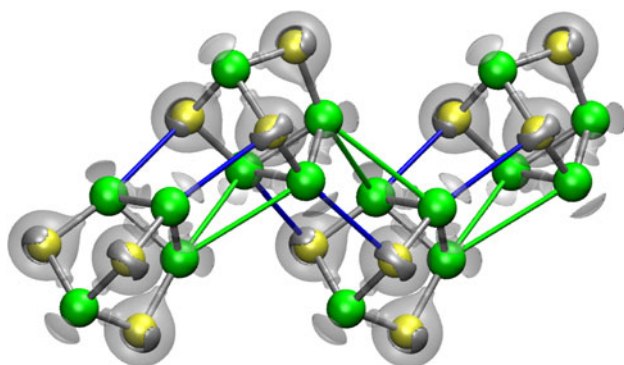


Fig. 17 A moiety of the structure of β -dimorphite displaying a string of As–As bonded interactions that parallels [100]. See legends of Figs. 9 and 10 for details

path lengths are 3.56 and 3.84 Å. The greater stability of α -dimorphite at room temperature may be ascribed to its larger number of the As–S bonded interactions relative to that observed for β -dimorphite.

Rigid body analysis for selected thioarsenide molecules

With the algorithms invented by Downs (2000), a rigid body analysis was completed for the As_4S_n molecules for the thioarsenides to learn the extent to which the thermal

energy of the molecules is consistent with the translational and librational motions of the molecules. If the bonded interactions are predominately isotropic, then the librational (angular oscillation) motion of the molecules may be expected to dominate the translational motion, whereas if the bonded interactions are directed, then the converse may be expected, with the translational motion dominating. Of the seven thioarsenides with As_4S_n molecules, the structures of only three (realgar, β -AsS and uzonite) were refined with anisotropic displacement parameters that indicated rigid body behavior. This means that the mean-square displacement parameters were approximately equal along the vector linking each pair of atoms within the molecule. The other structures either were not refined with anisotropic displacement parameters, or else their displacement parameters did not indicate rigid body motion, a result that may reflect a poor refinement or poor crystal quality.

The rigid body analysis for the As_4S_4 molecule in realgar (Kyono 2009) resulted in a librational angle of 4.9° , comparable with an angle of 5.4° calculated for the silicate SiO_4 tetrahedral oxyanion of low quartz at room temperature (Downs 2000). On the basis of the analysis and the fact that the silicate tetrahedra in quartz are linked by directed Si–O bonded interactions, it is apparent that the bonded interactions in realgar are directed to the extent that the bulk of the thermal energy ($\sim 85\%$) is associated with translational motion, and substantially less is associated with the angular oscillatory motion of the As_4S_4 molecules. However, in the case of the lower density, high temperature β -AsS polymorph (Burns and Percival 2001), the libration of the As_4S_4 molecule is different from that for the low temperature α -AsS polymorph (realgar), with a libration angle of 7.02° . As such, still 68% of the motion is translation, as may be expected given that it is high temperature polymorph of AsS. But, like realgar, the libration angle for the As_4S_5 molecule in uzonite is also comparable with that for quartz, 3.44° , with the bulk of the motion, 80%, being translational. Accordingly, on the basis of the rigid body analysis, the thermal energy of the molecules in realgar and uzonite is consistent with translational motion, the sort of motion that may be expected for molecular structures governed by lock and key directed bond paths.

Bond critical point and local-energy density properties

There are two types of As–S bonded interactions in the thioarsenides: the intramolecular As–S bond interactions (together with As–As bonded interactions discussed below) that bind the As and S together into molecules and directed intermolecular interactions that served to structuralize the molecules into periodic structures. The trend between the

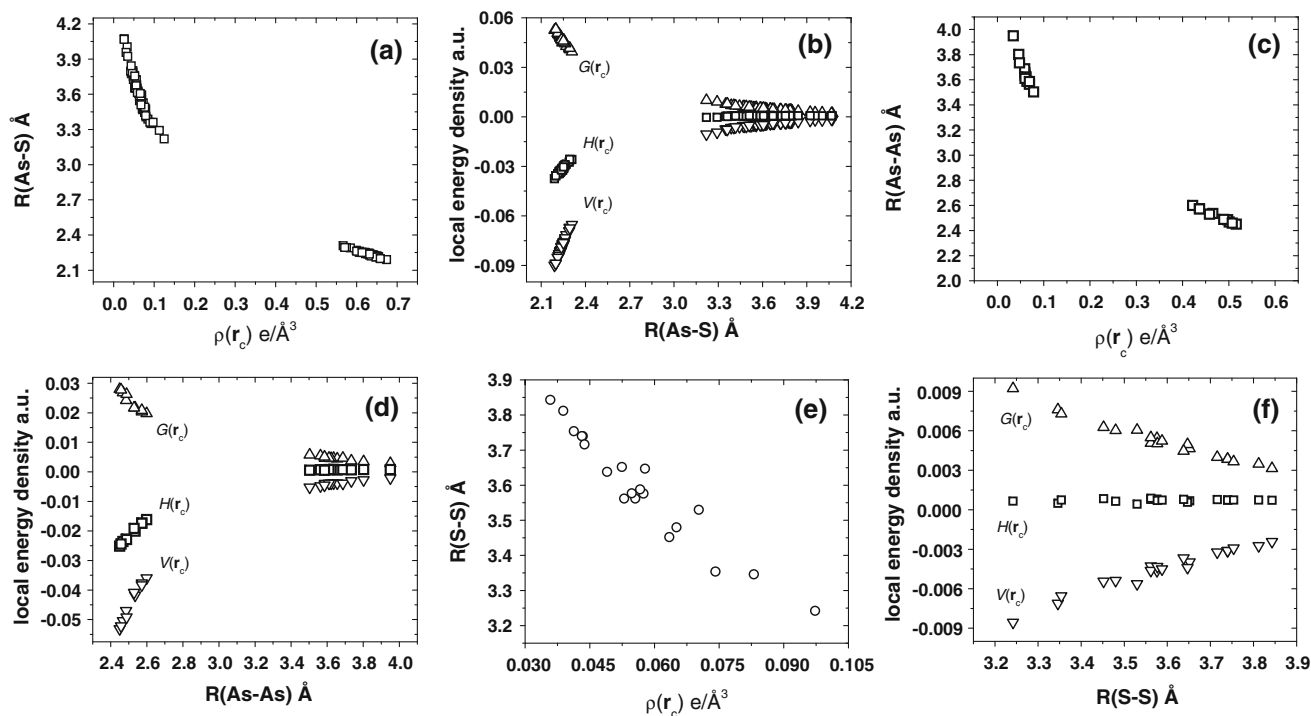


Fig. 18 Bond critical point and local-energy density properties calculated for the thioarsenides. **a** Scatter diagram of the As–S bond path lengths, $P(\text{As–S})$, plotted with respect to the value of the electron density at the bond critical point, $\rho(\mathbf{r}_c)$, **b** plotted with respect to the local-energy density properties $G(\mathbf{r}_c)$, $H(\mathbf{r}_c)$ and $V(\mathbf{r}_c)$. **c** Scatter diagram of the As–As bond path lengths, $P(\text{As–As})$, plotted with

respect to the value of the electron density at the bond critical point, $\rho(\mathbf{r}_c)$, **d** plotted with respect to the local-energy density properties $G(\mathbf{r}_c)$, $H(\mathbf{r}_c)$ and $V(\mathbf{r}_c)$. **e** Scatter diagram of the S–S bond path lengths, $P(\text{S–S})$, plotted with respect to the value of the electron density at the bond critical point, $\rho(\mathbf{r}_c)$, **f** plotted with respect to the local-energy density properties $G(\mathbf{r}_c)$, $H(\mathbf{r}_c)$ and $V(\mathbf{r}_c)$.

bond paths lengths for the As–S interactions, $P(\text{As–S})$, and the value of the ED at the bond critical point, $\rho(\mathbf{r}_c)$, is displayed in Fig. 18a. Clearly, the $\rho(\mathbf{r})$ values for the intramolecular bonded interactions are substantially greater than those for intermolecular bonded interactions. Despite the break in the trend between the $P(\text{As–S})$ and $\rho(\mathbf{r})$ values displayed by the inter- and the intramolecular populations, they seem to follow a common trend. The trend suggests that there is a continuum of bonded interaction between the shared and intermolecular bonded interactions as suggested by Slater (1972). About half of the $P(\text{As–S})$ are less $R_{\text{vdW}}(\text{As–S})$ indicating that a comparable number of As–S bond path lengths are less than the sum of the radii for As and S. As $\rho(\mathbf{r}_c)$ increases, sum decreases and the As and S atoms mutually penetrate one another, greater the strength of the interaction (Carroll and Bader 1988). The $\rho(\mathbf{r}_c)$ values for intermolecular and intramolecular bonded interactions in the thioarsenide molecular crystals alacránite, uzonite, realgar, β -AsS, pararealgar, α -dimorphite and β -dimorphite are given in Tables 1, 2, 3, 4, 5, 6 and 7, respectively.

The values of the positive definite local kinetic energy, $G(\mathbf{r}_c)$, the negative definite local potential energy density, $V(\mathbf{r}_c)$ and the local total energy density, $H(\mathbf{r}_c)$, are plotted

with respect to $P(\text{As–S})$, for the two populations shown in Fig. 18b. The $H(\mathbf{r}_c)$ values for the intermolecular bonded interactions cluster about the zero value and classify as close shell interactions. In contrast, as the values for intramolecular interactions are less than zero, they classify as shared interactions (Cremer and Kraka 1984) with the shared character of the bonded interactions increasing with decreasing bond length.

Like the As–S bonded interactions, there are two types of As–As bonded interactions: the intramolecular As–As interactions together with the As–S intramolecular that bind the atoms of the molecules and the intermolecular interactions that together with the As–S intermolecular interactions that bind the molecules of the crystals. Both the intramolecular and intermolecular As–As bond path lengths, $P(\text{As–As})$, decrease nonlinearly with $\rho(\mathbf{r})$ again with a break between the two populations (Fig. 18c). On the basis of the values of the local charge densities, the intramolecular bonded interactions qualify as shared interactions and the intermolecular interactions classify as closed-shell interactions (Fig. 18d). Furthermore, the shared character of the As–As bonded interaction increases with decreasing bond path length. It is noteworthy, that thioarsenides only contain S–S bonded intermolecular

Table 5 Bond paths for pararealgar (Bonazzi et al. 1995)

P (Å)	$\rho(\mathbf{r}_c)$ e/Å ³	x	y	z
As–S intramolecular bcp coordinates				
2.239	0.627	0.3902	−0.4184	0.1295
2.254	0.613	0.2438	−0.3265	0.1165
2.261	0.607	0.2595	−0.4558	0.0012
2.252	0.607	0.1235	−0.3738	0.2607
2.253	0.620	0.1653	−0.4880	0.4131
2.245	0.631	0.3138	0.4183	0.4225
2.228	0.632	0.4162	0.4423	0.2828
2.190	0.674	0.1708	0.3954	0.0627
As–As intramolecular bcp coordinates				
2.486	0.497	0.1153	0.4457	0.2414
2.535	0.465	0.2587	0.3547	0.2504
As–S intermolecular bcp coordinates				
3.475	0.079	0.2474	−0.2891	−0.1301
3.608	0.062	0.4249	−0.4412	−0.0836
3.794	0.047	0.2820	−0.1733	0.0352
3.388	0.085	−0.0565	−0.4548	0.1913
3.786	0.048	−0.0832	−0.4617	0.4237
3.619	0.059	0.2879	0.2067	0.3956
3.654	0.053	0.4546	0.1923	0.3140
3.594	0.070	0.1935	0.1838	0.0842
3.653	0.052	−0.0115	0.2754	0.2356
3.725	0.049	0.1812	0.3006	−0.1918
As–As intermolecular bcp coordinates				
3.802	0.046	0.4746	−0.2610	0.1026
3.656	0.059	0.0000	0.5000	0.5000
3.687	0.059	−0.0309	−0.3087	0.3340
S–S intermolecular bcp coordinates				
3.346	0.083	0.3898	0.4761	−0.3524
3.480	0.065	0.2129	−0.1303	0.1048

bonded interactions that, together with the As–S and As–As interactions, bind the molecules as crystals. Like the As–S and As–As bonded intermolecular interactions, $P(S-S)$ decreases in value with increasing $\rho(\mathbf{r})$ (Fig. 18e). As $H(\mathbf{r}_c)$ 0.0 for all of the interaction, the S–S interactions also qualify as closed-shell interactions (Fig. 18f).

Summarizing comments

The bulk of the thioarsenide molecules are linked by (1) intermolecular As–S bond paths that connect the Lewis-acid regions on the As atoms and Lewis-base regions on the S atoms, (2) As–As intermolecular bond path interactions that are comparable with the directed bonded interactions that bind the sheets of As atoms in bulk arsenic and (3) S–S intermolecular bond path interactions that are

Table 6 Bond Paths for α -dimorphite (Whitfield 1973a)

P (Å)	$\rho(\mathbf{r}_c)$ e/Å ³	x	y	z
As–S intramolecular bcp coordinates				
2.230	0.639	−0.3085	0.1686	0.0653
2.235	0.635	−0.4112	0.2500	0.1873
2.221	0.636	0.4508	0.2500	0.0456
2.218	0.639	−0.3668	0.1046	−0.1699
As–As intramolecular bcp coordinates				
2.468	0.501	0.4914	0.1800	−0.1877
2.488	0.489	−0.4211	0.2500	−0.2911
As–S intermolecular bcp coordinates				
3.468	0.072	−0.1613	0.2500	0.2339
3.956	0.031	−0.2595	0.0822	0.3133
3.671	0.053	−0.1842	−0.0232	0.0756
3.652	0.058	0.3570	0.4145	−0.0353
3.720	0.040	0.3052	0.3285	−0.2770
3.653	0.054	−0.4715	0.1896	0.4587
3.800	0.048	−0.4594	−0.0605	−0.2506

Table 7 Bond Paths for β -dimorphite (Whitfield 1970)

P (Å)	$\rho(\mathbf{r}_c)$ e/Å ³	x	y	z
As–S intramolecular bcp coordinates				
2.220	0.650	0.2280	0.2500	0.4158
2.220	0.649	0.3353	0.1498	−0.4879
2.212	0.648	0.0442	0.2500	0.4808
2.199	0.658	0.2357	0.0717	−0.3479
As–As intramolecular bcp coordinates				
2.450	0.516	0.0637	0.1639	−0.3629
2.458	0.508	0.1562	0.2500	−0.2806
As–S intermolecular bcp coordinates				
3.775	0.044	−0.4991	0.4014	0.4325
4.073	0.026	0.4783	0.2500	0.2789
3.526	0.073	0.4926	0.4312	−0.3150
4.004	0.034	−0.1732	0.4016	0.4967
3.753	0.049	0.0135	−0.0715	−0.3339
As–As intermolecular bcp coordinates				
3.585	0.069	0.3482	0.0810	0.3313
3.950	0.034	−0.1864	0.3076	−0.3167
S–S intermolecular bcp coordinates				
3.562	0.053	0.5000	0.0000	−0.5000
3.843	0.036	0.3658	−0.0927	−0.2625

comparable with those that bind the S₈ molecules in native sulfur, bond paths that are comparable with those reported for solid chlorine, arsenolite, s enarmontite and orpiment (Gibbs et al. 2010). In each case, the bond paths are consistent with Feynman's (1939) assertion that interactions result in ED being accumulated between the bonded atoms, the greater the accumulation, the shorter the bond path.

The As–S, S–S and As–As bond paths determined for the thioarsenides are expected particularly given that these bonded interactions have been established between the layers of the orpiment structure in a careful study of the low-frequency Raman rigid interlayer modes (Zallen and Slade 1974).

In effect, the vdW bonded intermolecular interactions linking the molecules in thioarsenide crystals are no different from directed intramolecular bonded interactions in crystals other than that they are typically weaker (Slater 1972). On the basis of these results, we assert that the periodic and ordered structures adopted by the molecules are structuralized by directed vdW bond paths, the As–S bonded interactions in particular, resulting in the bulk of the molecules adopting a distorted cheek-by-jowl close-packed arrangement, a conclusion that agrees with Kitai-gorodskii's (1955) assertion that in the case of inorganic crystals, directional forces are decisive. Moreover, according to the Makovicky and Mumme (1983) micelle model, the features ascribed to the domains of lone pair electrons for all of the atoms of the thioarsenide molecules are pictured as 'inverted lone electron pair micelles' directed outward into the intermolecular space (Makovicky 2006). The bond paths displayed for the thioarsenide molecular structures are consistent with this picture in that the molecules in the structures are linked by directed interactions and provide a theoretical basis for the micelle model (Moëlo et al. 2008). They are also consistent with the picture of the lone pair clad regions in such rod-layer materials as dadsonite, $\text{Pb}_{23}\text{Sb}_{25}\text{S}_{60}\text{Cl}$ (Makovicky et al. 2006b) and the suggested twinned structure of kirkiite, $\text{Pb}_{10}\text{Bi}_3\text{As}_3\text{S}_{19}$, associated with row aligned lone pair clad regions linked by closed-shell bonded interactions (Makovicky et al. 2006a). However, the lone pair electrons of the As atoms are well developed which does not appear to be consistent with the $L(\mathbf{r})$ features displayed in this study for arsenic. Further, the features described as micelles represent regions in a material that are delineated by intramolecular bond paths and possibly cross-linked by long-range Lewis acid–base intermolecular closed-shell bonded vdW interactions rather than by isotropic semi-classical dispersion or dipole–dipole interactions. In short, the definition of micelle does not contradict in any way with the network of vdW bond paths crossing its core parts or the network of crisscrossing paths of the intermicelle space of an inverted micelle.

A rigid body analysis for realgar and uzonite revealed that the bulk of the thermal energy is translational and comparable with that calculated for the silicate tetrahedron in quartz, a result that is consistent directional forces. Of the bonded interactions, the As–S interactions not only appear to be the strongest but the most directed interactions that correspond to intermolecular Lewis base–acid

chemical interactions that, in effect, stabilize the structures. Further, the bulk of the intermolecular As–S bond lengths are shorter than the corresponding vdW radii by a much as $\sim 0.30 \text{ \AA}$ in some cases. Further, the alignment of the bond paths with Lewis acid–base regions reported for the thioarsenides is asserted to represent a new class of long-range intermolecular vdW interactions that are encrypted in the $L(\mathbf{r})$ distribution. As observed in this report, knowledge of the paths for the arsenates and the thioarsenides provides an improved and useful construct for visualizing the arrangement of the molecules in three-space. It is also expected to promote our understanding of the properties, the crystal chemistry of the thioarsenides and the arsenates together with their interaction with water at the atomic level with the concomitant release into the environment of deadly toxins. Moreover, the experimental bonded interactions established between the layers of orpiment (Zallen et al. 1971) not only provide a compelling basis for the long-range Lewis acid–base-directed As–S, S–S and the As–As bond paths that connect the layers (Gibbs et al. 2010) but also a basis for the bond paths found in this study for the thioarsenide molecular crystals. Further, the close agreement between the phonon dispersion curves for trigonal selenium and the experimental force constants for the interchain bonded interactions (Hamilton et al. 1974) clearly demonstrates that the vdW interchain interactions are directed (Martin et al. 1976).

Finally, reactions between thioarsenide minerals and aqueous solutions have been shown to render thioarsenide aqueous species (Helz and Tossell 2008; Spycher and Reed 1989), species that may be expected to be associated with thioarsenide molecular species. The question is 'How will the thioarsenide aqueous species possibly aggregate in an aqueous solution under suitable conditions, form a thioarsenide nanoparticle and ultimately a molecular crystal?' On the basis of the information established in this study, it is anticipated that the surface of an aqueous thioarsenide species will be clad with regions of locally concentrated (a Lewis-base region) and locally depleted ED (a Lewis-acid region) (Fig. 9). Further, the species may be anticipated to form directed vdW bond paths that radiate into space when the molecule is approached by another aqueous molecule, like the burrs on a burdock (behaving like Velcro), but rather than catching on to fur and clothing, actually catching on to and forming directed bond paths that connect the acid and base regions of an approaching thioarsenide species. When in solution, the thioarsenide aqueous species will likely be coordinated by highly labile water molecules and other aqueous species, attaching and detaching from the Lewis acid and base sites. When another aqueous thioarsenide molecule approaches, Lewis acid–base vdW paths may be expected to develop and attract, possibly eliminating all the other aqueous species

with the loss of the labile water molecules so that thioarsenide molecules can form an oriented attachment. If continued, this attachment process may provide a growth mechanism for a thioarsenide nanoparticle and ultimately form a molecular crystal that maximizes the number of long-range Lewis acid–base vdW As–S bonded interactions together with the formation of S–S and As–As bond paths with the resulting directed bond paths structuralizing the molecules as a molecular crystal.

Acknowledgments The National Science Foundation and the US Department of Energy are thanked for supporting this study with Grants EAR-0609885 (N.L.R. and G.V.G.), EAR-0609906 (R.T.D.), and DE-FG02-97ER14751 (D.F.C.). K.M.R. acknowledges a grant from the US Department of Energy (DOE), Office of Basic Energy Sciences, Geoscience Division and computational facilities and support from the Environmental Molecular Sciences Laboratory (EMSL) at the Pacific Northwest National Laboratory (PNNL). The computations were performed in part at the EMSL at PNNL. The EMSL is a national scientific user facility sponsored by the US DOE Office of Biological and Environmental Research. PNNL is operated by Battelle for the DOE under contract DEAC06-76RLO 1830. GVG wishes to thank his good friend and colleague Professor Michael Hochella for reading a preliminary draft of the manuscript and contributing to the discussion of the growth mechanism for a thioarsenide molecular crystal that maximizes the number of long-range Lewis acid–base vdW As–S bonded interactions. He also wishes to thank Professors Richard F. W. Bader at McMaster University, Ontario, Canada and Vladimir Tsirelson at Mendeleev University of Chemical Technology, Moscow, Russia for useful discussions related to van der Waals bonded interactions. We also want to thank Professor Emil Makovicky at University of Copenhagen, Copenhagen, Denmark for his careful review of the manuscript, his suggested changes and his insightful comments on the connection between micelles and directed bond paths.

References

- Bader RFW (1990) *Atoms in molecules*. Oxford Science Publications, Oxford
- Bader RFW (1998) A bond path: a universal indicator of bonded interactions. *J Phys Chem A* 102(37):7314–7323
- Bader RFW (2009) Bond paths are not chemical bonds. *J Phys Chem A* 113(38):10391–10396
- Bader RFW (2010) Definition of molecular structure: by choice or by appeal to observation? *J Phys Chem A* 114(28):7431–7444
- Bader RFW, Essén H (1984) The characterization of atomic interactions. *J Chem Phys* 80(5):1943–1960
- Bader RFW, MacDougall PJ (1985) Toward a theory of chemical reactivity based on the charge density. *J Am Chem Soc* 107(24):6788–6795
- Bader RFW, MacDougall PJ, Lau CDH (1984) Bonded and nonbonded charge concentrations and their relation to molecular geometry and reactivity. *J Am Chem Soc* 106(6):1594–1605
- Bader RFW, Gillespie RJ, Macdougall PJ (1988) A physical basis for the VSEPR model of molecular-geometry. *J Am Chem Soc* 110(22):7329–7336
- Bader RFW, Hernandez-Trujillo J, Cortes-Guzman F (2007) Chemical bonding: from Lewis to atoms in molecules. *J Comput Chem* 28(1):4–14
- Ballirano P, Maras A (2006) In situ X-ray transmission powder diffraction study of the kinetics of the light induced alteration of realgar (alpha-As₄S₄). *Eur J Mineral* 18(5):589–599
- Bindi L, Popova V, Bonazzi P (2003) Uzonite, As₄S₅, from the type locality: single-crystal X-ray study and effects of exposure to light. *Can Mineral* 41:1463–1468
- Boese R, Boese AD, Blaser D, Antipin MY, Ellern A, Seppelt K (1997) The surprising crystal packing of chlorinefluoride. *Angew Chem Int Ed Engl* 36(13–14):1489–1492
- Bonazzi P, Bindi L (2008) A crystallographic review of arsenic sulfides: effects of chemical variations and changes induced by exposure to light. *Z Kristallogr* 223(1–2):132–147
- Bonazzi P, Menchetti S, Pratesi G (1995) The crystal-structure of pararealgar, As₄S₄. *Am Mineral* 80(3–4):400–403
- Bonazzi P, Bindi L, Popova V, Pratesi G, Menchetti S (2003) Alacranite, As(8)S(9): structural study of the holotype and re-assignment of the original chemical formula. *Am Mineral* 88(11–12):1796–1800
- Bone RGA, Bader RFW (1996) Identifying and analyzing intermolecular bonding interactions in van der Waals molecules. *J Phys Chem* 100(26):10892–10911
- Bozorth RM (1923) The crystal structures of the cubic forms of arsenious and antimonous oxides. *J Am Chem Soc* 45(7):1621–1627
- Bullen HA, Dorko MJ, Oman JK, Garrett SJ (2003) Valence and core-level binding energy shifts in realgar (As₄S₄) and pararealgar (As₄S₄) arsenic sulfides. *Surf Sci* 531(3):319–328
- Burns PC, Percival JB (2001) Alacranite, As₄S₄: a new occurrence, new formula, and determination of the crystal structure. *Can Mineral* 39:809–818
- Carroll MT, Bader RFW (1988) An analysis of the hydrogen-bond in BASE–HF complexes using the theory of atoms in molecules. *Mol Phys* 65(3):695–722
- Cremer D, Kraka E (1984) A description of the chemical bond in terms of local properties of electron density and energy. *Croat Chem Acta* 57(6):1259–1281
- Dovbeshko GI, Fesenko OM, Obraztsova ED, Allakhverdiev KR, Kaja AE (2009) Conformation analysis of nucleic acids and proteins adsorbed on single-shell carbon nanotubes. *J Struct Chem* 50(5):954–961
- Downs RT (2000) Analysis of harmonic displacement factors. In: Hazen RM, Downs RT (eds) *High-temperature and high-pressure crystal chemistry*, vol 41. Mineralogical Society of America, Washington, DC
- Dunitz JD, Gavezzotti A (2005) Molecular recognition in organic crystals: directed intermolecular bonds or nonlocalized bonding? *Angew Chem Int Ed Engl* 44(12):1766–1787
- Dunitz JD, Gavezzotti A (2009) How molecules stick together in organic crystals: weak intermolecular interactions. *Chem Soc Rev* 38(9):2622–2633
- Feldman K, Fritz M, Hahner G, Marti A, Spencer ND (1998) Surface forces, surface chemistry and tribology. *Tribol Int* 31(1–3):99–105
- Feynman RP (1939) Forces in molecules. *Phys Rev* 56(4):340
- Fiedler S, Broecker J, Keller S (2010) Protein folding in membranes. *Cell Mol Life Sci* 67(11):1779–1798
- French RH, Parsegian VA, Podgornik R, Rajter RF, Jagota A, Luo J, Asthagiri D, Chaudhury MK, Chiang YM, Granick S, Kalinin S, Kardar M, Kjellander R, Langreth DC, Lewis J, Lustig S, Wesolowski D, Wettlaufer JS, Ching WY, Finnis M, Houlihan F, von Lilienfeld OA, van Oss CJ, Zemb T (2010) Long range interactions in nanoscale science. *Rev Mod Phys* 82(2):1887–1944
- Gatti C (1997) TOPOND96 user's manual. CNR–CSRSRC, Milan
- Gibbs GV, Wallace AF, Cox DF, Dove PM, Downs RT, Ross NL, Rosso KM (2009) Role of directed van der Waals bonded interactions in the determination of the structures of molecular arsenate solids. *J Phys Chem A* 113(4):736–749
- Gibbs GV, Wallace AF, Zallen R, Downs RT, Ross NL, Cox DF, Rosso KM (2010) Bond paths and van der Waals interactions in orpiment, As₂S₃. *J Phys Chem A* 114(23):6550–6557

- Gotzinger M, Peukert W (2003) Dispersive forces of particle-surface interactions: direct AFM measurements and modelling. *Powder Technol* 130(1–3):102–109
- Hamilton WC, Lassier B, Kay MI (1974) Phonon spectra of trigonal selenium at 77 and 298 K. *J Phys Chem Solids* 35(9):1089–1094
- Helz GR, Tossell JA (2008) Thermodynamic model for arsenic speciation in sulfidic waters: a novel use of ab initio computations. *Geochim Cosmochim Acta* 72(18):4457–4468
- Hillier IH, Rice SA (1967) Comments on influence of intermediate excitons and exchange forces on interaction in molecular crystals—crystal structure of chlorine. *J Chem Phys* 46(10):3881–3889
- Ito T, Morimoto N, Sadanaga R (1952) The crystal structure of realgar. *Acta Crystallogr A* 5(6):775–782
- Kitaigorodskii AI (1955) Organic chemical crystallography. Academy of Sciences of USSR, Moscow
- Kitaigorodskii AI (1973) Molecular crystals and molecules. Academic Press, New York
- Kyono A (2009) Molecular conformation and anion configuration variations for As_4S_4 and As_4Se_4 in an anion-substituted solid solution. *Am Mineral* 94(4):451–460
- Kyono A, Kimata M, Hatta T (2005) Light-induced degradation dynamics in realgar: in situ structural investigation using single-crystal X-ray diffraction study and X-ray photoelectron spectroscopy. *Am Mineral* 90(10):1563–1570
- Lauria A, Ippolito M, Almerico AM (2009) Inside the Hsp90 inhibitors binding mode through induced fit docking. *J Mol Graph Model* 27(6):712–722
- Lichanot A, Apra E, Dovesi R (1993) Quantum-mechanical Hartree-Fock study of the elastic properties of Li_2S and Na_2S . *Physica Status Solidi B Basic Res* 177(1):157–163
- Maitland GC, Rigby M, Smith EB, Wakeham WA (1980) Intermolecular forces: their origin and determination. Oxford University Press, Oxford, 450 pp
- Makovicky E (2006) Crystal structures of sulfides and other chalcogenides. *Rev Mineral Geochem* 61(1):7–125
- Makovicky E, Mumme WG (1983) The crystal-structure of ramdohrite, $Pb_6Sb_{11}Ag_3S_{24}$, and its implications for the andorite group and zinckenite. *Neues Jahrb Mineral Abh* 147(1):58–79
- Makovicky E, Balic-Zunic T, Karanovic L, Poleti D (2006a) The crystal structure of kirkiite, $Pb_{10}Bi_3As_3S_{19}$. *Can Mineral* 44:177–188
- Makovicky E, Topa D, Mumme WG (2006b) The crystal structure of dadsonite. *Can Mineral* 44:1499–1512
- Martin RM, Lucovsky G, Helliwell K (1976) Intermolecular bonding and lattice-dynamics of Se and Te. *Phys Rev B* 13(4):1383–1395
- Mikami B, Degano M, Hehre EJ, Sacchetti JC (1994) Crystal-structures of soybean beta-amylase reacted with beta-maltose and maltal—active-site components and their apparent roles in catalysts. *Biochemistry* 33(25):7779–7787
- Mořlo Y, Makovicky E, Mozgova NN, Jambor JL, Cook N, Pring A, Paar W, Nickel EH, Graeser S, Karup-Moller S, Balic-Zunic T, Mumme WG, Vurro F, Topa D, Bindi L, Bente K, Shimizu M (2008) Sulfosalt systematics: a review Report of the sulfosalt sub-committee of the IMA Commission on Ore Mineralogy. *Eur J Mineral* 20(1):7–46
- Naumov P, Makreski P, Jovanovski G (2007) Direct atomic scale observation of linkage isomerization of As_4S_4 clusters during the photoinduced transition of realgar to pararealgar. *Inorg Chem* 46(25):10624–10631
- Nyburg SC (1964) Intermolecular Forces + Space Group of Solid Chlorine. *J Chem Phys* 40(9):2493–2501
- O'Day P (2006) Chemistry and mineralogy of arsenic. *Elements* 2(2):77–83
- Parr RG, Yang W (1989) Density-functional theory of atoms and molecules. Oxford University Press, Oxford, p 333
- Pine SH, Hendrickson JB (1980) Organic chemistry. McGraw-Hill, New York
- Saunders VR, Dovesi R, Roetti C, Causa M, Harrison NM, Orlando R, Apra E (1998) CRYSTAL98 user's manual. University of Torino, Torino
- Scherer W, Spiegler M, Pedersen B, Tafipolsky M, Hieringer W, Reinhard B, Downs AJ, McGrady GS (2000) Molecular recognition in the solid state: topology of experimental and theoretical charge densities for tetrasulfur tetranitride. *Chem Commun* (7):635–636
- Slater JC (1972) Hellmann-Feynman and virial theorems in the X alpha method. *J Chem Phys* 57(6):2389–2396
- Smedley PL, Kinniburgh DG (2002) A review of the source, behaviour and distribution of arsenic in natural waters. *Appl Geochem* 17(5):517–568
- Sponer J, Riley KE, Hobza P (2008) Nature and magnitude of aromatic stacking of nucleic acid bases. *Phys Chem Chem Phys* 10(19):2595–2610
- Spycher NF, Reed MH (1989) As(III) and Sb(III) sulfide complexes—an evaluation of the stoichiometry and stability from existing experimental data. *Geochim Cosmochim Acta* 53(9):2185–2194
- Thonhauser T, Cooper VR, Li S, Puzder A, Hyldgaard P, Langreth DC (2007) Van der Waals density functional: self-consistent potential and the nature of the van der Waals bond. *Phys Rev B* 76(12):125112-1–125112-11
- Towler MD, Dovesi R, Saunders VR (1995) Magnetic-interactions and the cooperative Jahn-Teller effect in $KCuF_3$. *Phys Rev B* 52(14):10150–10159
- Tsirelson VG, Zou PF, Tang TH, Bader RFW (1995) Topological definition of crystal-structure—determination of the bonded interactions in solid molecular chlorine. *Acta Crystallogr A* 51:143–153
- Tsirelson VG, Shishkina AV, Stash AI, Parsons S (2009) The experimental and theoretical QTAIMC study of the atomic and molecular interactions in dinitrogen tetroxide. *Acta Crystallogr B* 65(5):647–658
- Wei A, Tripp SL, Liu J, Kasama T, Dunin-Borkowski RE (2009) Calixarene-stabilised cobalt nanoparticle rings: self-assembly and collective magnetic properties. *Supramol Chem* 21(3–4):189–195
- Welch AH, Westjohn DB, Helsel DR, Wanty RB (2000) Arsenic in ground water of the United States: occurrence and geochemistry. *Ground Water* 38(4):589–604
- Whitfield HJ (1970) Crystal structure of tetra-arsenic trisulphide. *J Chem Soc* (10):1800–1803
- Whitfield HJ (1973a) Crystal and molecular-structure of tetra-arsenic pentasulfide. *J Chem Soc Dalton Trans* (17):1740–1742
- Whitfield HJ (1973b) Crystal-structure of beta-form of tetra-arsenic trisulfide. *J Chem Soc Dalton Trans* (17):1737–1738
- Whitten AE, Dittrich B, Spackman MA, Turner P, Brown TC (2004) Charge density analysis of two polymorphs of antimony(III) oxide. *Dalton Trans* (1):23–29
- Williams DE, Hsu LY (1985) Transferability of nonbonded Cl=Cl potential-energy function to crystalline chlorine. *Acta Crystallogr A* 41:296–301
- Xu J, Stevens MJ, Oleson TA, Last JA, Sahai N (2009) Role of oxide surface chemistry and phospholipid phase on adsorption and self-assembly: isotherms and atomic force microscopy. *J Phys Chem C* 113(6):2187–2196
- Zallen R, Slade M (1974) Rigid-layer modes in chalcogenide crystals. *Phys Rev B* 9(4):1627–1637
- Zallen R, Slade ML, Ward AT (1971) Lattice vibrations and interlayer interactions in crystalline As_2S_3 and As_2Se_3 . *Phys Rev B* 3(12):4257–4273